Thermodynamic model for mineral solubility in aqueous fluids: theory, calibration and application to model fluid-flow systems

D. DOLEJŠ[1,2] AND C. E. MANNING[1,3]

[1]*Bayerisches Geoinstitut, University of Bayreuth, Bayreuth, Germany;* [2]*Institute of Petrology and Structural Geology, Charles University, Praha, Czech Republic;* [3]*Department of Earth and Space Sciences, University of California Los Angeles, Los Angeles, CA, USA*

ABSTRACT

We present a thermodynamic model for mineral dissolution in aqueous fluids at elevated temperatures and pressures, based on intrinsic thermal properties and variations of volumetric properties of the aqueous solvent. The standard thermodynamic properties of mineral dissolution into aqueous fluid consist of two contributions: one from the energy of transformation from the solid to the hydrated-species state and the other from the compression of solvent molecules during the formation of a hydration shell. The latter contribution has the dimension of the generalized Krichevskii parameter. This approach describes the energetics of solvation more accurately than does the Born electrostatic theory and can be extended beyond the limits of experimental measurements of the dielectric constant of H_2O. The new model has been calibrated by experimental solubilities of quartz, corundum, rutile, calcite, apatite, fluorite and portlandite in pure H_2O at temperatures up to 1100°C and pressures up to 20 kbar. All minerals show a steady increase in solubility along constant geothermal gradients or water isochores. By contrast, isobaric solubilities initially increase with rising temperature but then decline above 200–400°C. This retrograde behavior is caused by variations in the isobaric expansivity of the aqueous solvent, which approaches infinity at its critical point. Oxide minerals predominantly dissolve to neutral species; so, their dissolution energetics involve a relatively small contribution from the solvent volumetric properties and their retrograde solubilities are restricted to a relatively narrow window of temperature and pressure near the critical point of water. By contrast, Ca-bearing minerals dissolve to a variety of charged species; so, the energetics of their dissolution reactions involve a comparatively large contribution from volume changes of the aqueous solvent and their isobaric retrograde solubility spans nearly all metamorphic and magmatic conditions. These features correlate with and can be predicted from the standard partial molar volumes of aqueous species.

The thermodynamic model can be used over much wider range of settings for terrestrial fluid–rock interaction than has previously been possible. To illustrate, it is integrated with transport theory to show quantitatively that integrated fluid fluxes characteristic of crustal shear zones are capable of precipitating quartz or calcite veins from low- and medium-grade metamorphic conditions, at a geothermal gradient of 20°C km^{-1}. For subduction zones, modeled by a geotherm of 7°C km^{-1}, the required fluid fluxes are one to two orders of magnitude lower and predict enhanced efficiency of mass transfer and metasomatic precipitation in comparison with orogenic settings. The new model thus can be applied to shallow hydrothermal, metamorphic, magmatic and subduction fluids, and for retrieval of dependent thermodynamic properties for mass transfer or geodynamic modeling.

Key words: density model, hydration, mass transfer, mineral solubility, thermodynamics

Received 24 August 2009; accepted 30 January 2010

Corresponding author: D. Dolejš, Institute of Petrology and Structural Geology, Charles University, 12843 Praha 2, Czech Republic.
Email: ddolejs@natur.cuni.cz. Tel.: +420-221 951 532. Fax: +420-221 951 533.

INTRODUCTION

Aqueous fluids play a fundamental role in mass and energy transfer in the Earth's interior. Fluids are produced by diagenetic and metamorphic devolatilization, and magmatic degassing in geodynamic settings ranging from mid-ocean ridges to convergent plate boundaries and collisional orogens (Fig. 1). In turn, they are responsible for mobility
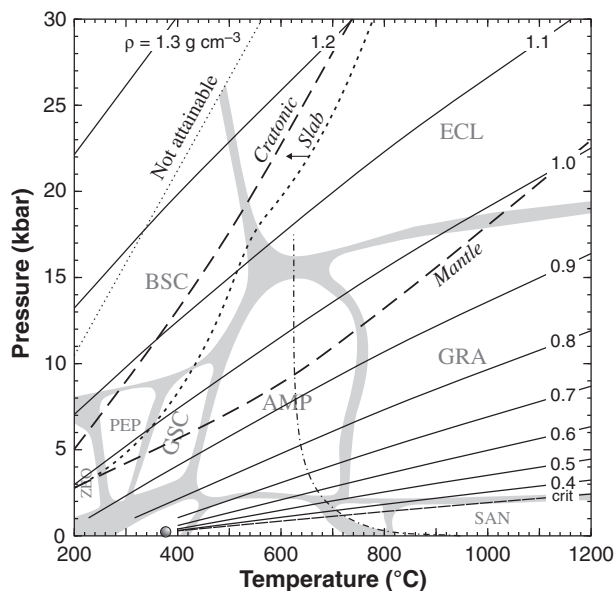
Fig. 1. Pressure–temperature diagram relating the metamorphic facies, beginning of the hydrous haplogranite melting (dot-dashed curve), representative geotherms (Vernon & Clarke 2008, their fig. 1.15), and isochores of H_2O calculated using the IAPWS 95 equation of state (Wagner & Pruß 2002). Abbreviations for metamorphic facies: AMP, amphibolite; BSC, blueschist; ECL, eclogite; GSC, greenschist; PEP, prehnite-pumpellyite; SAN, sanidinite; ZEO, zeolite facies.

and transport of inorganic and organic solid and liquid phases and gaseous non-electrolytes (Ague 1994, 2003; Jamtveit & Yardley 1997; Ferry & Gerdes 1998). The mass transfer is manifested by distinct element depletion–enrichment patterns in subduction-zone metamorphism and arc magmas (Scambelluri et al. 2004; Zack & John 2007), in metamorphic rocks and veins in convergent orogens (Widmer & Thompson 2001; Spandler & Hermann 2006), in alteration patterns and in ore-forming and contact metasomatic environments (Reed 1997; Mehnert et al. 2005) as well as in small-scale fluid-mediated dissolution–precipitation phenomena (Pina et al. 2004; Putnis & Putnis 2007). Many of these alteration styles are strongly non-isochemical, and this is corroborated by high time-integrated fluid fluxes, 10^1–10^6 m^3 m^{-2}, inferred for diffuse and focused flow and alteration (Ferry 1994; Thompson 1997; Ferry & Gerdes 1998; Ague 2003).

The thermodynamic properties of dissolved aqueous species at elevated temperatures and pressures are most frequently described by the Helgeson–Kirkham–Flowers model (Helgeson et al. 1981; Tanger & Helgeson 1988; Shock et al. 1992). In this formulation, the thermodynamic state functions of an aqueous species consist of a solvation contribution, defined by the Born (1920) theory, and empirical heat capacity and volumetric contributions, which also include anomalous solute–solvent interactions at low temperatures (Angell 1983). This model provides a

versatile tool for modeling mass transfer up to 5 kbar (Johnson et al. 1992; Oelkers et al. 1995); however, it suffers from several deficiencies: (i) it is only applicable at liquid-like density of H_2O, $\rho > 0.322$ g cm^{-3} to 1000°C and 5 kbar; (ii) it cannot accurately reproduce the derivative properties in the vicinity of the critical point of H_2O; (iii) it becomes particularly inaccurate for gaseous non-electrolytes at their low-density limit (Plyasunov et al. 2000; Akinfiev & Diamond 2003); (iv) the static permittivity of water, which is required for the Helgeson–Kirkham–Flowers equation of state, has not been determined experimentally at $T > 600$°C or $P > 20$ kbar, and current models strongly diverge in these regions (Franck et al. 1990; Shock et al. 1992; Wasserman et al. 1995, Fernandéz et al. 1997; Marshall 2008a).

In contrast to the static permittivity, the volumetric properties of H_2O are known with reasonable accuracy at nearly all conditions of terrestrial water–rock interaction. Simple extrapolation schemes and more advanced models based on H_2O volumetric properties have been successful in representing association–dissociation equilibria (Franck 1956a; Marshall & Quist 1967; Mesmer et al. 1988; Anderson et al. 1991; Plyasunov 1993), element partitioning in vapor–liquid systems (Pokrovski et al. 2005a, 2008), dissolution of gaseous species in aqueous fluids (Plyasunov et al. 2000; Akinfiev & Diamond 2003), mineral solubilities over a wide range of temperatures and pressures in aqueous solvents (Fournier & Potter 1982; Manning 1994; Pokrovski et al. 2005b), extrapolation to mixed solvents (Marshall 2008b; Akinfiev & Diamond 2009) and describing near-critical thermodynamic properties of inorganic and organic solutes (Clarke et al. 2000; Sedlbauer & Wood 2004; Majer et al. 2008).

In this paper, we investigate the thermodynamic relationships between mineral solubility, solvent density and other intensive variables, with the main focus on metamorphic and magmatic temperatures and pressures. The 'density model' will be derived from the thermodynamics of solute hydration, emphasizing consistency with conventional caloric properties and thermodynamic parameters resulting from statistical mechanics of solute–solvent interactions. This optimized functional form is shown to serve for interpolation and extrapolation of mineral solubilities in aqueous fluids at high temperatures and pressures, as well as for retrieving the thermodynamic properties of dissolution that are necessary for mass transfer and transport modeling.

THERMODYNAMIC MODEL

Thermodynamic properties of hydration, which result from electrostatic interactions between solute species and aqueous solvent, have traditionally been described by the Born theory (Born 1920; Helgeson & Kirkham 1974; Wood

et al. 1981, 1994; Atkins & MacDermott 1982; Pitzer 1983b; Tanger & Helgeson 1988; Tremaine *et al.* 1997), which states that

$$\Delta_{B} G = \omega \frac{1}{\varepsilon}, \qquad (1)$$

where $\Delta_{B} G$ is the Born energy, ω is the species-specific Born parameter and ε is static permittivity (dielectric constant) of the aqueous solvent. However, the reciprocal dielectric constant varies nearly linearly with temperature at constant water density at 200–1100°C and up to 10 kbar (Fig. 2). The linear trend corresponds to

$$\frac{1}{\varepsilon} = -4.928 \times 10^{-4} T \log \rho_{w} + 3.497 \times 10^{-2} \qquad (2)$$

where T is absolute temperature (K) and ρ_{w} is water density (g cm^{-3}). Consequently, the electrostatic contribution can be, to a high degree of accuracy, implicitly accounted for via correlations with solvent density. Such an approach would alleviate a number of drawbacks due to: (i) lack of calibration of the static permittivity at high temperatures and pressures (cf. Pitzer 1983b; McKenzie & Helgeson 1984; Franck *et al.* 1990; Shock *et al.* 1992; Wasserman *et al.* 1995; Fernández *et al.* 1997) and (ii) inadequate representation by Born theory of near-critical and low-pressure thermodynamic properties (Tanger & Pitzer 1989a; Shock *et al.* 1992; Plyasunov *et al.* 2000; Sue *et al.* 2002; Akinfiev & Diamond 2003, 2004), where formulations based on solvent density are more accurate (Fournier 1983, Manning 1994; Plyasunov *et al.* 2000; Sedlbauer *et al.* 2001; Sedlbauer & Wood 2004; Majer *et al.* 2008).
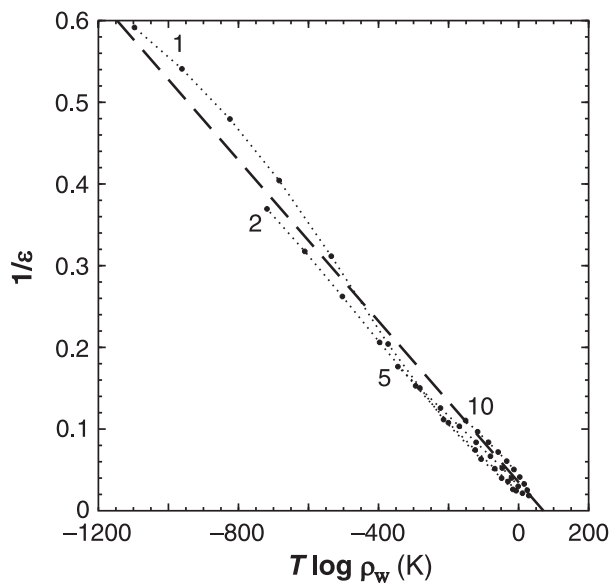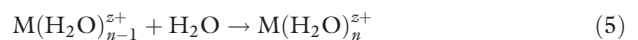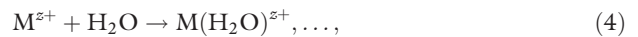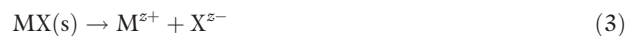

Fig. 2. Correlation between the reciprocal dielectric constant of H$_2$O, $1/\varepsilon$, and the $T \log \rho$ term illustrated for isobars of 1, 2, 5 and 10 kbar (labels of dotted curves) at a temperature range of 200–1100°C (point symbols in 100°C steps). Dashed line is a linear fit of the set (Eq. 2).

An alternative thermodynamic model can be formulated by accounting for three thermodynamic contributions to mineral dissolution into an aqueous fluid. At a given temperature and pressure, these are: (i) disruption of local structure of the crystal lattice, (ii) hydration of the solute species and (iii) volumetric solute–solvent interactions resulting from electrostriction. These contributions are added in a Born–Haber thermodynamic cycle to derive the standard thermodynamic properties of dissolution.

Lattice breakdown and hydration

The first two steps in the dissolution process – disruption of solid phase MX and formation of hydrated aqueous species – are represented by a series of chemical equilibria (cf. Kebarle 1977; Pitzer 1983a; Borg & Dienes 1992, pp. 126–137), e.g. for ion M(H$_2$O)$_n^{z+}$:

$$MX(s) \rightarrow M^{z+} + X^{z-} \qquad (3)$$

$$M^{z+} + H_2O \rightarrow M(H_2O)^{z+}, \ldots, \qquad (4)$$

$$M(H_2O)_{n-1}^{z+} + H_2O \rightarrow M(H_2O)_n^{z+} \qquad (5)$$

where n represents hydration number. Equations similar to 3–5 also apply to negatively charged species, ion pairs and neutral complexes. The standard Gibbs energy change of the two combined steps is described at the pressure of interest by a caloric (cl) equation of state:

$$\Delta_{cl} G = \Delta H + \int_{T_{ref}}^{T} c_P \, dT - T \left(\Delta S + \int_{T_{ref}}^{T} \frac{c_P}{T} dT \right) \qquad (6)$$

where T and T_{ref} represent the temperature of interest and reference temperature (e.g. 298.15 K) respectively. An explicit PV term is not required here because the standard state is chosen to be that at the pressure of interest and the volumetric contribution will be included in a density term, as shown below. When the heat capacity, c_P, is a polynomial linear in temperature, which appears to be sufficient to represent the properties of aqueous species up to high temperatures (Pitzer 1982; Tanger & Pitzer 1989a,b; Holland & Powell 1998), Eq. 6 leads upon substitution and integration to the following Gibbs function:

$$\Delta_{cl} G = a + bT + cT \ln T + dT^2 \qquad (7)$$

where the coefficients a to d are related to enthalpy, entropy and the heat capacity polynomial (Hillert 2008, pp. 407–408).

Volumetric solute–solvent interactions

Additional thermochemical contributions arise from volumetric collapse (electrostriction) of the hydration shell. The contribution to the Gibbs energy corresponds to the

PV work required to compress H_2O molecules from the bulk solvent (w) density to that in the hydration shell (hs) (Pierotti 1963, 1976; Ben-Naim 2006, pp. 12),

$$\Delta_{co}G = \Delta_{w \to hs}G = RT \ln \frac{V_w}{V_{hs}} = RT \ln \frac{\rho_{hs}}{\rho_w} \qquad (8)$$

where the subscript 'co' stands for compression, and V and ρ are the molar volume and density at each state respectively. Assuming negligible compressibility of the hydration shell, that is, ρ_{hs} is constant (Mesmer *et al.* 1988; Tanger & Pitzer 1989a), Eq. 8 introduces two terms to the overall Gibbs energy of dissolution – an $RT \ln \rho_{hs}$ term, where $R \ln \rho_{hs}$ has dimension of entropy, and an $RT \ln \rho_w$ term, which varies with temperature and pressure. Note that the $T \ln \rho_w$ product has the same form as the term in the proposed correlation for the reciprocal dielectric constant (Eq. 2).

Differentiation of $\Delta_{co}G$ (Eq. 8) with respect to pressure provides the standard molar volume change during the formation of the hydration shell,

$$\Delta_{co}V = \left(\frac{\partial \Delta_{co}G}{\partial P} \right)_T = -\beta_w RT, \qquad (9)$$

where β_w is the compressibility of H_2O (cf. Mesmer *et al.* 1988; Anderson *et al.* 1991; Ben-Amotz *et al.* 2005). This form has an independent origin in fluctuation solution theory, which defines linear scaling between the standard partial molar volume of aqueous species, V_{aq}, and the solvent compressibility as the generalized Krichevskii parameter, A (Levelt Sengers 1991; O'Connell *et al.* 1996; Plyasunov *et al.* 2000):

$$A = \frac{V_{aq}}{\beta RT}. \qquad (10)$$

The function $1 - A$ is complementary to the generalized Krichevskii parameter and represents the dimensionless spatial integral of the infinite-dilution solute–solvent direct-correlation function (Kirkwood & Buff 1951; O'Connell 1971, 1990). It has the advantage of behaving as a finite smooth function in the vicinity of the critical point and it is nearly independent of temperature when applied to both electrolyte and non-electrolyte systems (Cooney & O'Connell 1987; Crovetto *et al.* 1991). The constant relationship between the solute partial molar volume and the solvent compressibility has, in addition, been confirmed experimentally up to elevated temperatures for inorganic solutes in aqueous and organic solvents (Hamann & Lim 1954; Ellis 1966).

MODEL FOR MINERAL DISSOLUTION

The energetic terms associated with lattice breakdown (dissociation) and solute hydration ($\Delta_{cl}G$, Eq. 7), and with

solvent compression ($\Delta_{co}G$, Eq. 8) including solute–solvent interactions, are summed to give the standard Gibbs energy of dissolution, $\Delta_{ds}G$:

$$\Delta_{ds}G = \Delta_{cl}G + \Delta_{co}G \qquad (11)$$

leading to

$$\Delta_{ds}G = a + bT + cT \ln T + dT^2 + eT \ln \rho, \qquad (12)$$

which represents the standard reaction Gibbs energy of equilibria such as SiO_2 (quartz) = SiO_2 (aq) or CaF_2 (fluorite) = Ca^{2+} (aq) + $2F^-$ (aq). In Eq. 12, a to e are parameters of the model. Parameters c and d represent the constant and the linear terms in the heat capacity of dissolution respectively; where experimental data are sparse, these terms may be set to zero. As discussed below, the reduced three-parameter form (a, b and e) is sufficient to represent data that extend over at least 400°C. An explicit term representing the intrinsic volume of species is not required for the properties of dissolution when the hard-core volumes of ions in the lattice and in the hydration sphere are assumed to be comparable.

Using the relationship between the standard reaction Gibbs energy and equilibrium constant, K,

$$0 = \Delta_{ds}G + RT \ln K, \qquad (13)$$

Eq. 12 leads to

$$\ln K = -\frac{1}{R} \left\{ \frac{a}{T} + b + c \ln T + dT + e \ln \rho_w \right\}. \qquad (14)$$

Equation 14 indicates that there is an isothermal linear dependence of the logarithm of the equilibrium constant on the logarithm of solvent density, and that this linear slope is independent of temperature. Dissolution and association–dissociation equilibria at elevated pressures indeed appear to conform to a simple linear relationship including a logarithmic term of the solvent density,

$$\log K = m + n \log \rho_W, \qquad (15)$$

where m and n are fit parameters, which are often empirical polynomial expansions in temperature (Mosebach 1955; Franck 1956a; Marshall & Quist 1967; Mesmer *et al.* 1988; Anderson *et al.* 1991). Such a behavior is characteristic of the dissociation of water up to 1000°C and 10 kbar (Sweeton *et al.* 1974, Marshall & Franck 1981; Fig. 3A), the dissociation of alkali halides up to 800°C and 4 kbar (Franck 1956b; Quist & Marshall 1968; Frantz & Marshall 1982; Fig. 3B), the dissociation of acids and bases (Eugster & Baumgartner 1987; Mesmer *et al.* 1988, 1991; Tremaine *et al.* 2004) and the dissolution of quartz, calcite, apatite, halite and other minerals up to 900°C and 20 kbar (Mosebach 1955; Franck 1956b; Martynova 1964; Fournier & Potter 1982; Manning 1994;
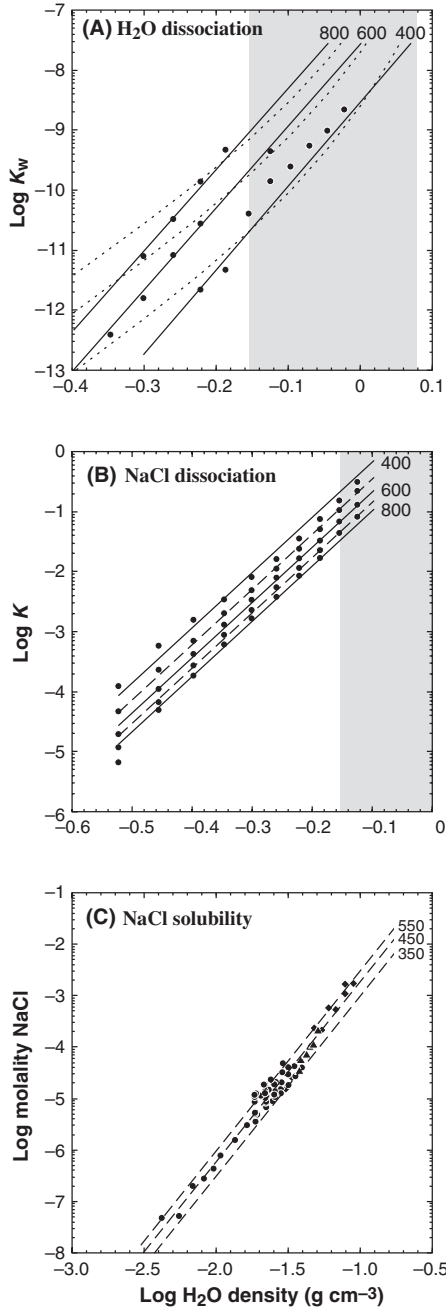
Fig. 3. Linear relationships between logarithmic density of aqueous solvent and logarithmic equilibrium constants for homogeneous solvent and salt dissociation, and salt solubility: (A) Self-dissociation of H_2O with experimental data at liquidlike densities. Solid lines represent the fit of Marshall & Franck (1981), dotted curves are the model of Bandura & Lvov (2006), and point symbols are experimental data from Quist (1970), at 400, 600 and 800°C. (B) Dissociation of NaCl (aq). Experimental data by Quist & Marshall (1968) are shown by point symbols at 400, 500, 600, 700 and 800°C, with isotherms fitted to the data set. (C) Halite solubility in aqueous vapor. Experimental measurements are indicated by the following symbols – circles: Galobardes et al. (1981); diamonds: Armellini & Tester (1993); triangles: Higashi et al. (2005). Dashed lines are isotherms at 350, 450 and 550°C fitted to the data set.

Caciagli & Manning 2003; Antignano & Manning 2008a; Fig. 3C).

The solubility model represented by Eqs 12 and 14 differs from previous empirical density models. The first part (*a–d* terms) has frequently been used with inverse temperature factors (e.g. Fournier & Potter 1982; Mesmer *et al.* 1988, 1991; Anderson *et al.* 1991). Such a Gibbs energy function is, however, inconsistent with a constant heat capacity term (cf. Hillert 2008, pp. 407–408) and we prefer a rigorous combination of enthalpy, entropy and heat capacity contributions. Similarly, the $\ln \rho$ term was used with either no or inverse temperature dependence (e.g. Fournier & Potter 1982; Mesmer *et al.* 1988, 1991; Holland & Powell 1998), which may, in part, simplify the macroscopic relationship between the solute volume and heat capacity (Anderson *et al.* 1991; Anderson 2005, pp. 260–263). However, these forms prevent extrapolation of thermodynamic properties above approximately 300°C (Anderson *et al.* 1991). Therefore, Anderson *et al.* (1991) and Holland & Powell (1998) proposed a modification, essentially a scaled $T \ln \rho_w$ term, in order to improve and extend the applicability to 800°C. This modification is fortuitously identical in form to the model that we derived using the compression of H_2O in the hydration sphere.

Thermodynamic identities lead to the standard thermodynamic properties of dissolution, as follows:

$$\Delta_{ds} S = -\left(\frac{\partial \Delta_{ds} G}{\partial T}\right)_P = -b - c(1 + \ln T) - 2dT \\ - e \ln \rho_w + eT\alpha_w, \tag{16}$$

$$\Delta_{ds} H = \Delta_{ds} G + T\Delta_{ds} S = a - cT - dT^2 + eT^2 \alpha_w, \tag{17}$$

$$\Delta_{ds} c_P = -T\left(\frac{\partial^2 \Delta_{ds} G}{\partial T^2}\right)_P = -c - 2dT + 2eT\alpha_w + eT^2\left(\frac{\partial \alpha_w}{\partial T}\right)_P, \tag{18}$$

$$\Delta_{ds} V = -\left(\frac{\partial \Delta_{ds} G}{\partial P}\right)_T = eT\beta_w, \tag{19}$$

$$\Delta_{ds} \beta = -\frac{1}{\Delta_{ds} V}\left(\frac{\partial \Delta_{ds} V}{\partial P}\right)_T = -eT\left(\frac{\partial \beta_w}{\partial P}\right)_T, \tag{20}$$

where ρ_w, α_w and β_w represent the density, isobaric expansivity and isothermal compressibility of the solvent respectively.

These thermodynamic relationships can also be used for deriving model parameters for a solubility equilibrium of interest by using the $\Delta_{ds} H$, $\Delta_{ds} S$ and $\Delta_{ds} V$ or $\Delta_{ds} c_P$ at reference temperature and pressure (e.g. 25°C and 1 bar) from existing thermodynamic databases (e.g. Wagman *et al.* 1982; Johnson *et al.* 1992; Oelkers *et al.* 1995; Parkhurst & Appelo 1999; Hummel *et al.* 2002). The calculation procedure for a three-parameter version of the model is given in Appendix A.

The new thermodynamic model (Eq. 12) suggests a functional form for a stand-alone equation of state for aqueous species. Any arbitrary standard thermodynamic property, Υ, of bulk aqueous solute (aq) is a combination of corresponding property of dissolving solid phase (s) and its change during dissolution:

$$\Upsilon(\text{aq}) = \Upsilon(\text{s}) + \Delta_{ds}\Upsilon. \tag{21}$$

An equation of state for a solid phase and the standard thermodynamic properties of dissolution (Eq. 12, 16–18 or 19) can thus be added to obtain an equation of state for aqueous solutes applicable at high temperatures and pressures, which will consist of a caloric term (enthalpy, entropy and a heat capacity polynomial), a volumetric term (intrinsic volume of the species) and a density term.

CALIBRATION OF THE MODEL

Solubilities of seven simple minerals – three oxides (quartz, corundum and rutile) and four calcium-bearing phases (anhydrite, apatite, calcite and fluorite) – have been determined experimentally at high temperatures and pressures and were used to explore the model and evaluate its performance. These minerals dissolve both as neutral or charged aqueous species, and their solubilities differ by seven orders of magnitude. For the solvent properties, we

have employed the equation of state of H_2O for scientific use (Harvey 1998; Wagner & Pruß 2002), which is calibrated by experiments to 1 GPa but extrapolates reasonably to very high pressures. Experimental solubility data at elevated pressure and temperature were first converted to molal concentration of the solute, temperature and density of H_2O; multiple experiments at the same pressure and temperature were averaged to a single value in order to avoid artificial weighting of the fit. The reduced data sets were fitted by linear least squares to the equation of state for dissolution (Eq. 14). The resulting model parameters are listed in Table 1, standard thermodynamic properties at 25°C and 1 bar are presented in Table 2 and the results plotted in Figs 4 and 5.

The solubility of quartz in aqueous fluids and fluid mixtures has been extensively studied from ambient conditions up to 1100°C and 20 kbar (e.g. Manning 1994 and references therein, Newton & Manning 2008a) and evaluated by Walther & Helgeson (1977), Fournier & Potter (1982), Manning (1994), Akinfiev (2001) and Gerya et al. (2005). We have calibrated our thermodynamic model using a subset of direct-sampling or rapid-quench experimental data (Hemley et al. 1980; Walther & Orville 1983; Manning 1994) augmented by calculated values from Fournier & Marshall (1983). The five-parameter fit (Table 1) reproduces experimental data set from 25 to 900°C and from saturation vapor pressure up to 20 kbar

Table 1 Parameters of the thermodynamic model (Eqs 12, 14 and 16–20).

	a (kJ mol^{-1})	b (J K^{-1} mol^{-1})	c (J K^{-1} mol^{-1})	d (J K^{-2} mol^{-1})	e (J K^{-1} mol^{-1})	Data sources
Apatite-F	63.4 (11.6)	3.90 (10.83)			−89.32 (8.95)	1
Calcite	57.4 (7.6)	−35.71 (8.55)			−72.98 (6.83)	2, 3
Corundum	80.3 (5.9)	−29.31 (5.72)			−37.01 (2.82)	4, 5
Fluorite	56.4 (5.0)	−24.89 (4.92)			−59.73 (3.89)	6
Portlandite	13.1 (2.8)	10.05 (4.99)			−94.74 (3.47)	7
Quartz	23.6 (1.5)	−52.92 (34.9)	10.93 (5.46)	−0.0463 (0.0044)	−18.52 (0.27)	8–11
Rutile	104.0 (5.1)	−33.72 (4.88)			−13.32 (3.77)	12

The model parameters are consistent with equilibrium constant defined on the molal concentration scale (Eq. 14). Values in parentheses are 1 standard error. Sources of experimental data – 1: Antignano & Manning (2008a); 2: Fein & Walther (1989); 3: Caciagli & Manning (2003); 4: Becker et al. (1983); 5: Tropper & Manning (2007a); 6: Tropper & Manning (2007b); 7: Walther (1986); 8: Hemley et al. (1980); 9: Fournier & Marshall (1983); 10: Walther & Orville (1983); 11: Manning (1994); 12: Antignano & Manning (2008b).

Table 2 Standard thermodynamic properties of dissolution at T = 25°C and P = 1 bar.

	log K	$\Delta_{ds}G$ (kJ mol^{-1})	$\Delta_{ds}H$ (kJ mol^{-1})	$\Delta_{ds}S$ (J K^{-1} mol^{-1})	$\Delta_{ds}c_P$ (J K^{-1} mol^{-1})	$\Delta_{ds}V$ (cm^3 mol^{-1})
Apatite-F	−11.31 (0.09)	64.53 (0.49)	61.24	−11.02	−90.13	−12.08
Calcite	−8.20 (0.22)	46.78 (1.27)	55.69	29.90	−73.65	−9.87
Corundum*	−12.54 (0.15)	71.60 (0.83)	79.46	26.37	−37.35	−5.00
Fluorite	−8.59 (0.11)	49.01 (0.60)	55.01	20.13	−60.27	−8.07
Portlandite	−2.82 (0.09)	16.08 (0.53)	10.84	−17.60	−95.60	−12.81
Quartz	−3.91 (0.02)	22.32 (0.13)	24.05	5.80	−2.04	−2.50
Rutile	−16.45 (0.05)	93.93 (0.27)	103.98	33.72	−13.43	−1.80

*Properties metastable with respect to gibbsite. Thermodynamic properties are referred to the molality concentration scale. Values in parentheses represent 1 standard error on the fit over the whole range of temperature and pressure. Comparison with experimental solubilities not used in regression reveals errors of 1 kJ for $\Delta_{ds}G$ and 3 kJ for $\Delta_{ds}H$, respectively, at 25°C and 1 bar for quartz (Rimstidt 1997).
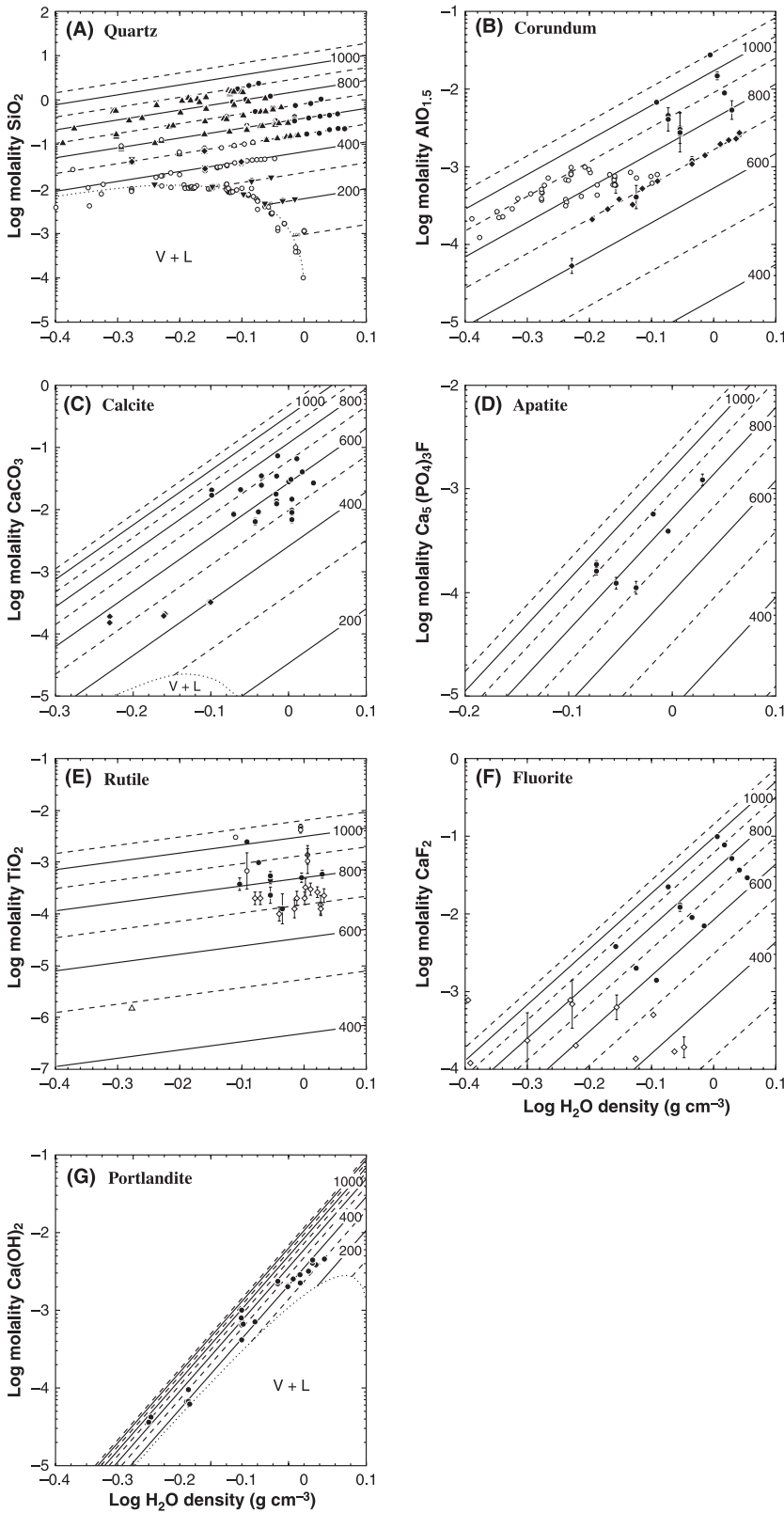
Fig. 4. Solubilities of rock-forming minerals in pure H_2O, expressed on the molality scale, and their changes with the H_2O density. Isotherms of solubility are calculated using the thermodynamic model (Eq. 14, Table 1), fitted to experimental data shown by filled symbols at selected temperatures and the liquid–vapor coexistence curve (experimental studies illustrated in open symbols were not used in fitting). Sources of experimental data – (A) solid upright triangles: Anderson & Burnham (1965); solid inverted triangles: Hemley *et al.* (1980); solid diamonds: Walther & Orville (1983); solid circles: Manning (1994); open circles: Kennedy (1950), Morey & Hesselgesser (1951), Wyart & Sabatier (1955), Kitahara (1960), Morey *et al.* (1962), Weill & Fyfe (1964), Crerar & Anderson (1971), at isotherms of 25, 100–900°C; (B) solid diamonds: Becker *et al.* (1983) at 666–700°C; solid circles: Tropper & Manning (2007a) at 700, 800, 900, 1000 and 1100°C; open circles: Walther (1997) at 400, 500 and 600°C; (C) solid diamonds: Fein & Walther (1989) at 400, 500 and 600°C; solid circles: Caciagli & Manning (2003) at 500, 600 and 700°C; (D) solid circles: Antignano & Manning (2008a) at 700, 800 and 900°C; (E) solid circles: Antignano & Manning (2008b) at 800, 900 and 1000°C; open circles: Tropper & Manning (2005) at 1000 and 1100°C; open diamonds: Audétat & Keppler (2005) at 821–1025°C; open triangle: Ryzhenko *et al.* (2006) at 500°C; (F) solid circles: Tropper & Manning (2007b) at 600, 700, 800, 900 and 1000°C; open diamonds: Strübel (1965) at 200, 300, 400, 500 and 600°C; (G) solid circles: Walther (1986) at 300, 400, 500 and 600°C. The V + L represents subcritical coexistence of aqueous liquid and vapor. Calculated solubilities in this and subsequent figures are extended into metastable regions where some phases may either transform (e.g. portlandite to portlandite II), hydrate (e.g. corundum to boehmite or gibbsite) or melt (e.g. calcite at $T > 750$°C).
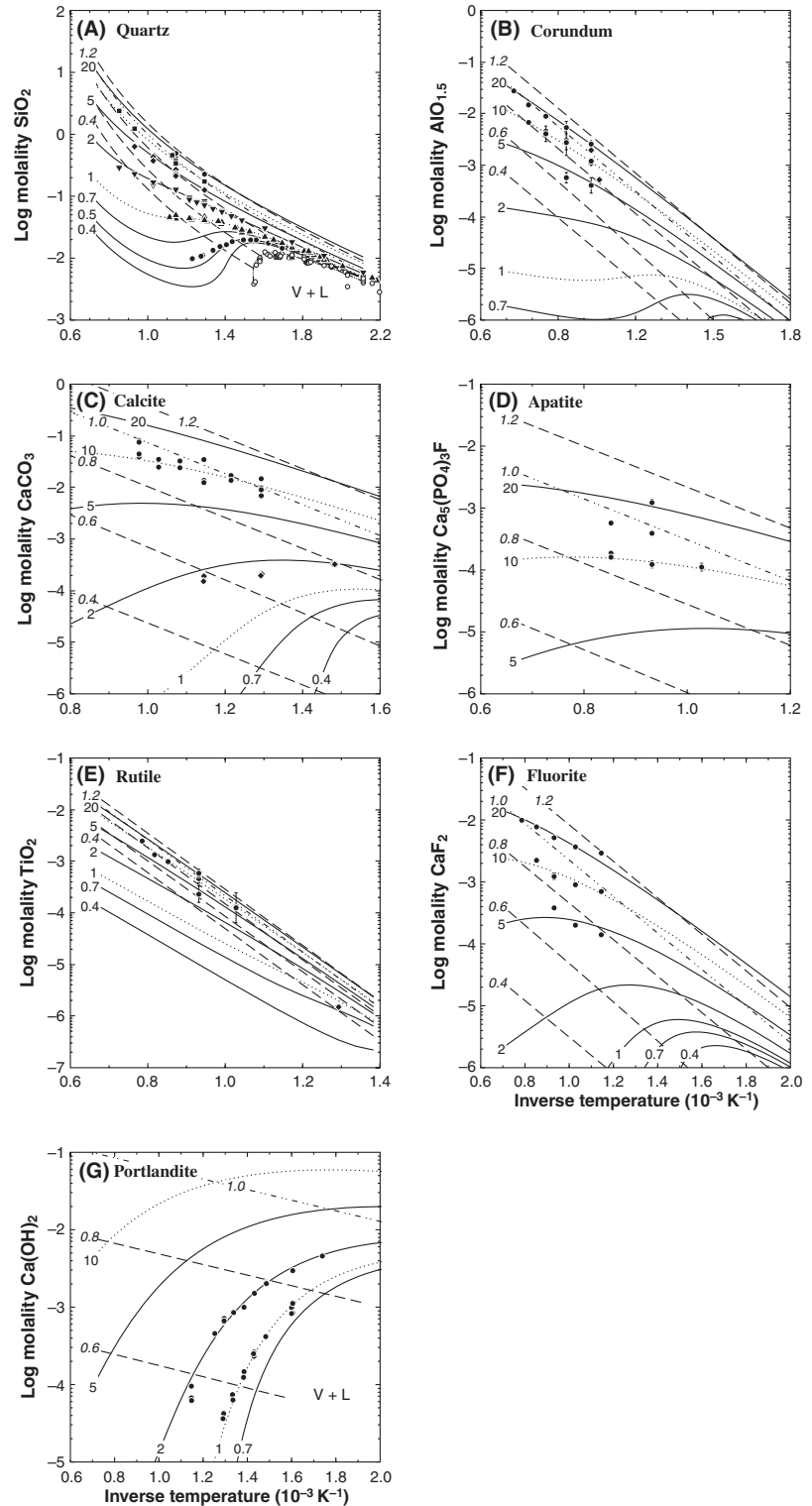
Fig. 5. Solubilities of rock-forming minerals in pure H_2O as a function of inverse absolute temperature. Isobars of solubility are indicated by solid and dotted curves, respectively, and labeled in upright numerals (pressure in kbar), whereas isochores are drawn by dashed and dot-dashed curves, respectively, and labeled in italic numerals (H_2O density in g cm^{-3}). Experimental solubility measurements are plotted along selected isobars and the liquid–vapor coexistence curve – (A) open circles: liquid–vapor coexistence curve; solid circles: 0.5 kbar; upright triangles: 1 kbar; inverted triangles: 2 kbar; diamonds: 5 kbar; squares: 10 kbar; hexagons: 20 kbar (Kennedy 1950; Morey & Hesselgesser 1951; Kitahara 1960; Morey *et al.* 1962; Weill & Fyfe 1964; Anderson & Burnham 1965; Crerar & Anderson 1971; Hemley *et al.* 1980; Walther & Orville 1983; Manning 1994); (B) diamonds: Becker *et al.* (1983) at 5, 10 and 20 kbar; circles: Tropper & Manning (2007a) at 10 and 20 kbar; (C) diamonds: Fein & Walther (1989) at 2 kbar; circles: Caciagli & Manning (2003) at 10 kbar; (D) circles: Antignano & Manning (2008a) at 10, 15 and 20 kbar; (E) diamond: Ryzhenko *et al.* (2006) at 1 kbar; circles: Antignano & Manning (2008b) at 10 and 20 kbar.

with remarkable accuracy (Figs 4A and 5A). In most cases, the scatter of multiple experiments exceeds the deviation between the experimental and calculated solubilities.

Despite the small data subset ($n = 84$) used in fitting the model, other experimental data are reproduced remarkably well (Fig. 5), with average deviation $\sigma = 0.017$, 5.23%.

Corundum solubilities in pure H_2O were experimentally determined by Becker *et al.* (1983), Ragnarsdóttir & Walther (1985), Walther (1997) and Tropper & Manning (2007a). The measurements of Becker *et al.* (1983) and Tropper & Manning (2007a) at 660–1100°C and 2.5–20 kbar are very consistent mutually and in their temperature and pressure dependencies (Figs 4B and 5B). The two studies of Walther and coworkers differ by log molality unit at $\rho_{H_2O} > 0.5$ g cm^{-3}. Careful examination of the data reveals that isothermal solubilities of Walther (1997) have a very similar dependence on the solvent density as those of Becker *et al.* (1983) and Tropper & Manning (2007a), but his reported solubilities are systematically greater by 1.2–1.5 log molality units. This suggests formation of additional Al-bearing complexes in Walther's (1997) experiments. Consequently, our thermodynamic model was fitted with experimental solubilities of Becker *et al.* (1983) and Tropper & Manning (2007a). The set of experiments ($n = 24$) is satisfactorily reproduced ($\sigma = 0.092$, 3.12%) with the reduced, three-parameter form of the model, $\ln K = -1/R(a/T + b + e \ln \rho)$, of the model (Table 1).

Rutile dissolves in pure H_2O to form neutral hydroxyspecies but is characterized by extremely low solubility. Neglecting an early study of Ayers & Watson (1993), which reported anomalously high solubilities due to mass transport in experiments, the rutile solubility has been experimentally determined by Tropper & Manning (2005), Audétat & Keppler (2005), Ryzhenko *et al.* (2006) and Antignano & Manning (2008b). These studies cover a temperature range of 500–1100°C at pressures of 1–20 kbar, and are complemented by low-temperature investigations of Vasilev *et al.* (1974), Zemniak *et al.* (1993) and Knauss *et al.* (2001) between 100 and 300°C and up to 200 bar. Earlier measurements of Tropper & Manning (2005) are associated with high analytical uncertainties and limited to temperatures of 1000–1100°C. By contrast, the diamond-anvil cell determinations by Audétat & Keppler (2005) gave consistently lower titanium concentrations and much lower dependence on temperature. A three-parameter fit to the data at 700–1000°C and 7–20 kbar of Antignano & Manning (2008b) ($n = 8$, $\sigma = 0.028$, 0.85%) reproduces rutile solubilities determined by fluid extraction at 500°C and 1 kbar (Ryzhenko *et al.* 2006) and 300°C and 200 bar (Knauss *et al.* 2001), respectively, to 0.2 log molality units (Fig. 4E).

Calcite dissolves congruently in pure water, and its solubility has been experimentally determined at high temperatures and pressures by Walther & Long (1986), Fein & Walther (1989) and Caciagli & Manning (2003), in addition to exploratory studies of Schloemer (1952) and Morey (1962). The solubilities reported by Walther & Long (1986) are 0.3–0.5 log molality units lower than subsequent measurements of Fein & Walther (1989) and were, therefore, discarded. The experimental results of Fein & Walther (1989) and Caciagli & Manning (2003) show

consistent and continuous behavior from 400 to 750°C and from 2 to 16 kbar, and were satisfactorily described by a three-parameter model ($n = 21$, $\sigma = 0.159$, 9.28%) to the thermodynamic model (Figs 4C and 5C).

Apatite solubility, using nearly pure fluorapatite (Durango, Mexico) comes from a single study of Antignano & Manning (2008a) at 700–900°C and 10–20 kbar ($n = 6$). Individual experimental measurements show consistent isothermal linearity in the $\log \rho$ versus $\log m$ space (Fig. 4D) and were fitted to a three-parameter model with $\sigma = 0.050$, 1.34%.

Fluorite solubility in pure water has been investigated by Strübel (1965) at 150–620°C up to 2.1 kbar and by Tropper & Manning (2007b) at 600–1000°C and 5–20 kbar. The earlier experiments are associated with very large analytical uncertainties and show no clear temperature dependence. By contrast, the recent measurements of Tropper & Manning (2007b) have high precision and display systematic variations with temperature and solvent density. This data set ($n = 12$) has been used for calibrating a three-parameter model fit ($\sigma = 0.086$, 3.84%).

Walther (1986) determined the solubility of portlandite in pure H_2O. Although the pressure–temperature range was smaller than for the other minerals considered here, the data were included in this study for several comparative purposes: (i) portlandite produces basic solution with high ionic strength, (ii) the data set covers a temperature range of 300–600°C, where significant changes in speciation are expected to occur and (iii) solubilities show a strong negative temperature dependence. As shown in Figs 4G and 5G, the experimental data ($n = 34$) are very well reproduced by a three-parameter fit to the thermodynamic model ($\sigma = 0.087$, 1.82%), which extends and confirms its application to systems with substantial changes in dissociation and variable ionic strength.

DISCUSSION

We fitted the experimental solubilities of seven minerals in pure water to a thermodynamic model (Eq. 14). The fitted experimental data cover a temperature range of 100–1100°C at pressures up to 20 kbar. The solubilities vary by up to six orders of magnitude on the molality concentration scale and are reproduced by the model to better than 5%, or 0.1 log molality units. Larger deviations, such as for calcite, are related not to the functional form of the thermodynamic model but rather to the scatter of repeated experiments at the same temperature and pressure or to poor consistency of different experimental or analytical methods.

The solubilities of six minerals were reproduced satisfactorily by a three-parameter function only, whereas quartz solubility required two additional terms to describe the heat capacity of the dissolution reaction and its linear dependence on temperature. It is noteworthy that quartz is

the most soluble mineral in our data set and that solute silica is known to polymerize (Zotov & Keppler 2000, 2002; Newton & Manning 2002, 2003, 2008a). In our model, aqueous silica reflects total dissolved silica in an unspecified but implicit mixture of monomeric and polymerized species. As the equilibrium constant for the homogeneous polymerization equilibrium is temperature dependent (Newton & Manning 2003; Manning *et al.* 2010), the heat capacity term – required to fit experimental data over an extended temperature range – presumably incorporates differences in enthalpies and entropies of the monomer and dimer, respectively, as their proportions in the bulk solute change with increasing temperature and pressure.

The isothermal, isobaric, isochoric and vapor-saturation solubilities presented in Figs 4 and 5 provide insights into interpolation and predictive capabilities of the new thermodynamic model, and illustrate the controls of aqueous speciation on these trends. In all cases, the mineral solubilities increase with the H_2O density at constant temperature (Fig. 4). The magnitude of this increase, $(\partial \log m/\partial \log \rho)_T$, depends on parameter e only, i.e. it is dictated by the combination of the generalized Krichevskii and Born parameter of the solute species. Quartz, corundum and rutile, which congruently dissolve as neutral hydroxyspecies at neutral conditions, e.g. $Si(OH)_4$, $Al(OH)_3$ and $Ti(OH)_4$ (Walther & Helgeson 1977; Bourcier *et al.* 1993; Knauss *et al.* 2001), show a relatively small increase in solubility with increasing water density at constant temperature, $(\partial \log m/\partial \log \rho)_T = 1.6–4.5$. By contrast, the solubilities of Ca-bearing minerals – calcite, apatite, fluorite and portlandite – exhibit much stronger dependence on the water density, $(\partial \log m/\partial \log \rho)_T = 7.2–11.4$. These phases involve congruent dissolution to a variety of charged species, ion pairs and neutral complexes (e.g. Ca^{2+}, CO_3^{2-}, HCO_3^-, OH^-, F^-, CaF^+, $H_2PO_4^-$, etc.; Walther 1986; Shock & Helgeson 1988; Fein & Walther 1989). The charged species cause much stronger electrostriction effects in the hydration shell as illustrated by the dependence of the species Helgeson–Kirkham–Flowers Born parameter on species charge (Shock & Helgeson 1988; Sverjensky *et al.* 1997). This translates to partial molar volumes of dissolution that grow more negative with increasing charge of the solute species. Using Eq. 19 at 25°C and 1 bar, the partial molar volumes of dissolution for quartz, corundum and rutile are $−1.8$ to $−5.0$ cm^{-3} mol^{-1}, whereas those for Ca-bearing phases are $−8.1$ to $−12.8$ cm^{-3} mol^{-1}. Consequently, electrostriction in the vicinity of the charged species promotes the solubility increase with pressure by a factor of three to four.

The spacing of isotherms in Fig. 4, $(\partial \log m/\partial T)_\rho$, varies between 7.7×10^{-3} and 6.1×10^{-2} and 5.9×10^{-4} and 4.7×10^{-3} K^{-1} at 25 and 800°C, respectively, and $\rho = 1$ g cm^{-3}. These variations are related to caloric properties in our model (Eq. 14) as follows:

$$\left(\frac{\partial \ln K}{\partial T}\right)_\rho = \frac{1}{R}\left\{\frac{a}{T^2} - \frac{c}{T} - d\right\}. \tag{22}$$

Equation 22 demonstrates that an increase in mineral solubility with temperature at constant density is free of hydration–compression effects. The caloric terms of all minerals broadly overlap at 25°C, but quartz, corundum and rutile are more endothermic at 800°C. Consequently, solubilities of these three minerals increase by a greater degree with temperature than that of the Ca-bearing minerals along isochores (cf. Fig. 1). This behavior is related either to distinct lattice enthalpies of oxides versus other minerals considered in this study, or to variably endothermic nature of chemical hydration of neutral versus charged aqueous species.

The changes in mineral solubilities with temperature at constant pressure are depicted in Fig. 5. The solubility isobars are highly nonlinear and often show retrograde solubility effects. The slope

$$\left(\frac{\partial \ln K}{\partial (1/T)}\right)_P = -\frac{\Delta_{ds} H}{R} \tag{23}$$

corresponds to the standard enthalpy of dissolution, which consists of caloric and volumetric contributions (Eq. 17). The caloric term is quasilinear or, more often, constant (when $c = d = 0$). By contrast, the volumetric term scales by parameter e in the model and is responsible for the reversals of solubility isobars as temperature changes. The solvent contribution to the enthalpy (Eq. 17) depends on the isobaric expansivity of H_2O, α, which is low, $0.5–2.0 \times 10^{-3}$ K^{-1} at low and high temperatures, respectively, but it diverges to infinity at the critical point of H_2O. This feature is inherited as a maximum in the expansivity versus temperature at supercritical pressures until it disappears at approximately 8 kbar (Helgeson & Kirkham 1974; Fletcher 1993, p. 221). As a consequence, the $e\alpha_w T^2$ term in Eq. 17 becomes very negative as the expansivity approaches its maximum. Depending on the magnitude of e, the expansivity term may counteract the positive caloric contribution $(a - cT - dT^2)$, leading to negative enthalpy of dissolution and hence mineral solubility that decreases with temperature at the highest values of α. The magnitude of this effect increases towards the critical point of H_2O.

The onset and extent of the isobaric retrograde solubility is directly related to the parameter e of the density term, i.e. it depends on the generalized Krichevskii and Born parameters of aqueous solute (Fig. 6A). For Ca-bearing minerals, the isobaric retrograde solubility appears from low- to medium-grade metamorphic temperatures and covers the high-temperature space through the granulite facies (Figs 6 and 7). The remarkable offset of the
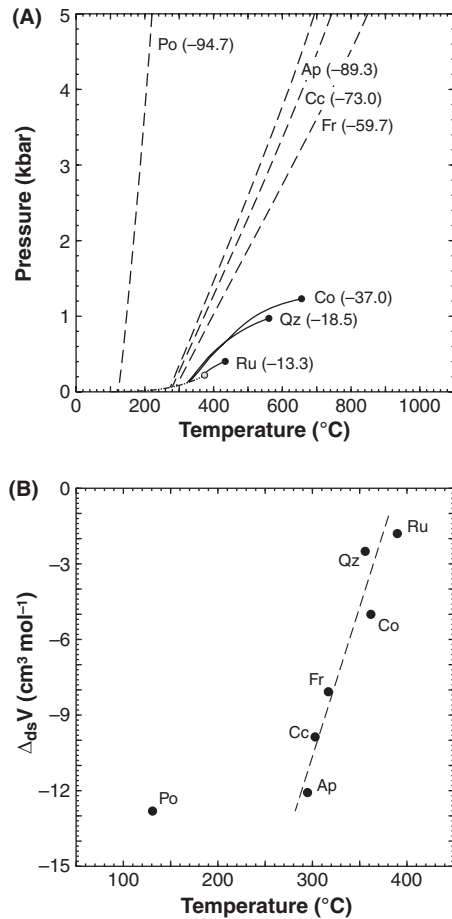
Fig. 6. Correlations between the isobaric retrograde solubility and its onset, and (A) model parameter *e* (numerical labels), which scales the solvent density, and (B) partial volume of dissolution (per mole of solute at *T* = 25°C and *P* = 1 bar) versus the onset of isobaric retrograde solubility (at *P* = 300 bar).

retrograde solubility of portlandite is due to its unusually low-standard enthalpy of dissolution (Table 2). By contrast, retrograde solubility behavior is suppressed where mineral dissolution produces neutral solutes, due to their very low electrostriction volumes (Table 2). Thus, for oxide minerals, retrograde solubility is more restricted in the pressure–temperature space (Fig. 7), and for the oxides considered in this study is limited to low pressures (rutile: 403 bar, quartz: 972 bar, corundum: 1231 bar).

GEOLOGICAL APPLICATIONS

We illustrate the performance and application of the thermodynamic model by evaluating the mineral solubilities in aqueous fluids along representative geotherms and by applying transport theory to assess mass transfer and fluid flux associated with model metasomatic scenarios.

Mineral solubilities along geothermal gradients

The calibrated thermodynamic model (Table 1, Eq. 14) allows the calculation of mineral solubilities at geothermal gradients of interest, chosen here as 20°C km^{-1} approximating the Barrovian continental gradient and 7°C km^{-1}, which corresponds to a representative subducting slab geotherm (cf. Fig. 1). In order to express the results in comparable quantities (ppm, wt% solute or vol% mineral), mass amounts of minerals have been recalculated to volumes using volumetric properties summarized in Table 3. The density of water has been calculated using the equation of state of Wagner & Pruß (2002), consistent with the model.

Figure 8 shows that mineral solubilities in aqueous fluids vary by 10 orders of magnitude, from sub-ppb to greater than 10 wt%. For all minerals except portlandite, the solubilities regularly increase with increasing depth along both gradients. The solubility increases by three to seven orders of magnitude between 200 and 1100°C. Although the portrayal using temperature as the independent variable (Fig. 8) shows little difference between the continental and the slab gradients, respectively, the limits of the diagram correspond to different pressures and depths. The observed trends are in agreement with general rule that mineral solubilities are mainly dependent on temperature. The calculations also imply that substantial changes in the solubilities are expected around thermal disturbances, e.g. magma chambers, emplaced at a given depth.

The sequence of minerals in Fig. 8 starts with quartz and calcite, followed by portlandite, fluorite, and apatite, whereas corundum and rutile are the least soluble and mobile phases in pure H$_2$O. These predictions are in good agreement with observed or inferred element mobilities during crustal fluid flow (e.g. Ague 2003). Titanium and aluminum solubilities are quite low in pure H$_2$O at all conditions. While this nominally supports their use as immobile elements in mass transfer, hydrothermal alteration and ore deposit studies (Maclean 1990; Maclean & Barrett 1993; Ague 1994; Dolejš & Wagner 2008), it is important to note that both elements may form soluble complexes with other elements (alkalies, halogens, silica, etc.) which can cause them to be mobilized in certain metasomatic environments (e.g. Tagirov & Schott 2001; Manning 2007; Manning *et al.* 2008; Newton & Manning 2008b).

Mineral solubilities at constant pressure

Mineral solubilities at constant pressure allow investigation of the potential for element mobility along flow paths associated with thermally induced gradients at a fixed crustal level, such as out- and inflow accompanying cooling of intrusions (Norton & Knight 1977; Hanson 1992;
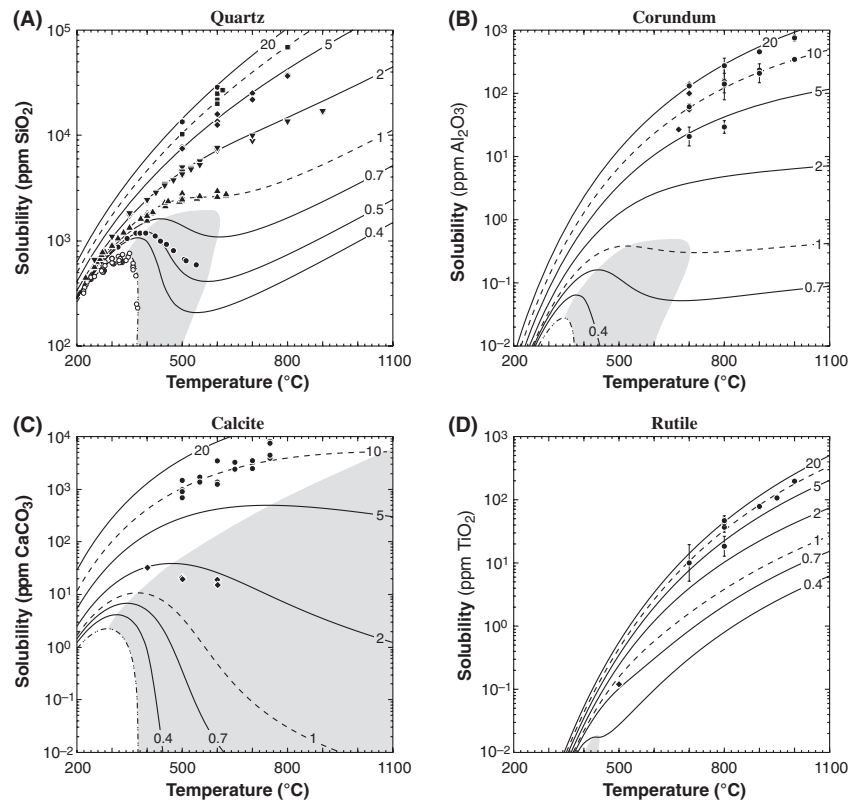
Fig. 7. Retrograde solubility behavior illustrated for (A) quartz, (B) corundum, (C) calcite and (D) rutile. Gray shading indicates regions where the isobaric mineral solubility decreases with increasing temperature. Experimental data and symbols are as in Fig. 5.

Table 3 Volumetric properties of minerals.

	V (cm³ mol⁻¹)	$\partial V/\partial T \times 10^5$ (cm³ K⁻¹ mol⁻¹)	$\partial V/\partial P \times 10^6$ (cm³ bar⁻¹ mol⁻¹)	Data sources
Apatite-F	157.14	12.24*	−5.38*	1
Calcite	36.59	12.24	−5.38	2
Corundum	25.37	6.70	−1.21	2
Fluorite	23.30	41.97	−10.15	3
Portlandite	32.25	19.14*	−5.11*	4
Quartz	22.55	11.03	−5.21	2
Rutile	18.65	5.33	−1.00	2

*Estimate obtained by correlation with similar substance. Molar volume of mineral at temperature and pressure of interest is defined by: $V_{P,T} = V + (\partial V/\partial T)T + (\partial V/\partial P)P$ where temperature, T, is in kelvin and pressure, P, in bar. Sources of data – 1: Mackie & Young (1974); 2: Holland & Powell (1998), updated in 2004 and available from the Thermocalc website (Richard White, University of Mainz); 3: Speziale & Duffy (2002); 4: Megaw (1933).

Norton & Dutrow 2001). Figure 9 compares predicted isobaric temperature dependence of mineral solubilities at 1 and 10 kbar respectively. With the exception of portlandite, the 10 kbar mineral solubilities and their temperature dependencies are very similar to those along geothermal gradients (Fig. 8); however, in detail, the magnitude of solubility increase above approximately 700°C is lower. Portlandite solubility declines with rising temperature. These features are a consequence of the larger decrease in H₂O density with temperature than along the geotherms.

The solubility behavior changes dramatically at low pressures, e.g. 1 kbar (Fig. 9B), as is expected from the variations in isobaric expansivity of H_2O. Rutile, which has the smallest parameter e is above its retrograde maximum, and its solubility increases monotonously with temperature. Quartz and corundum show a solubility plateau above 500°C; hence, mass transfer will be minimized at these conditions. The solubilities of Ca-bearing phases substantially decrease above 350–450°C; that of portlandite shows a steady decline over the whole temperature range. These results imply that temperature gradients in isobaric aquifers may alone be responsible for substantial decoupling of mineral precipitation and dissolution. The Ca-bearing minerals all dissolve as the fluid cools down to approximately 400°C, and the precipitation of, for instance, calcite or fluorite will be suppressed until temperature declines to below 350°C. This may explain a generally late nature of carbonate precipitation in hydrothermal ore veins (Mangas & Arribas 1987) or low temperatures of fluorite–barite mineralization (Baatartsogt *et al.* 2007). By contrast, quartz and aluminosilicate alteration reactions are predicted to experience a reversal (cf. Fournier & Potter 1982; Fournier 1999), i.e. mineral precipitation at magmatic and low temperatures, separated by a dissolution gap at near-critical conditions (cf. Fig. 7A, B). This mechanism has been postulated for the formation of quartz veins and desilicification in plutonic environments (Nichols & Wiebe 1998).
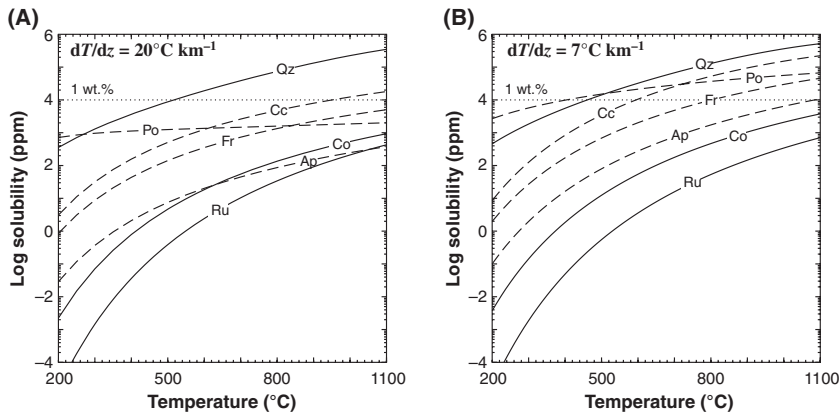
Fig. 8. Solubilities of rock-forming minerals in pure H_2O along geothermal gradients of (A) 20 and (B) 7°C km^{-1}. Solubilities of oxides are shown by solid curves whereas Ca-bearing phases are in dashed style.
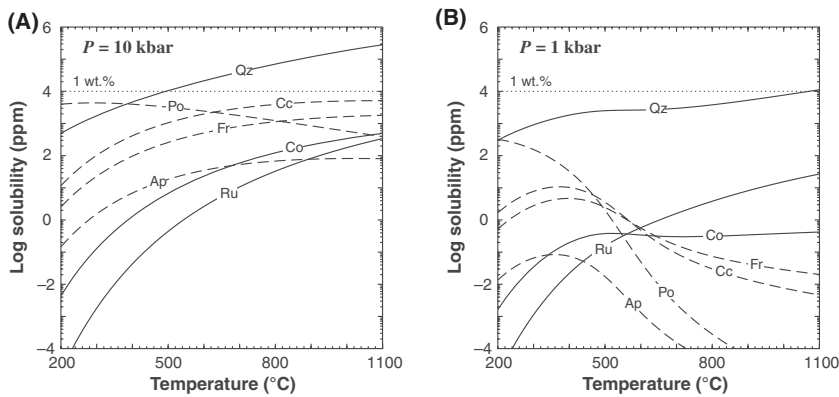

Fig. 9. Solubilities of rock-forming minerals in pure H_2O at constant pressure of (A) 10 and (B) 1 kbar. Line styles are as in Fig. 8.
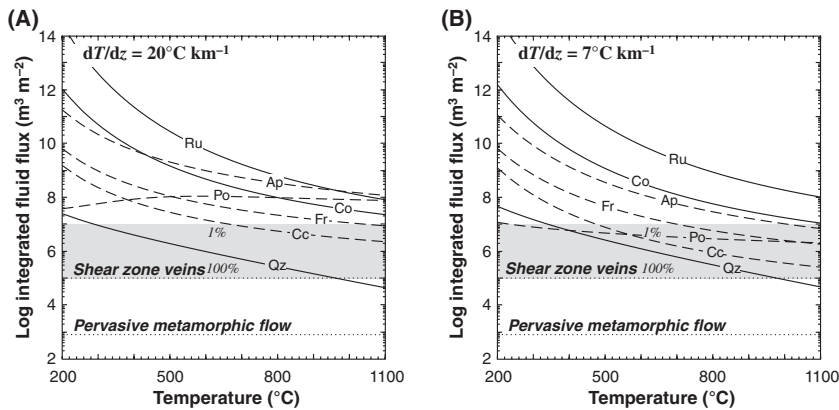

Fig. 10. The time-integrated fluid flux necessary to precipitate mineral vein filling (1 m^3) as a function of temperature along geothermal gradients of (A) 20 and (B) 7°C km^{-1}. Typical integrated fluid fluxes for diffuse metamorphic fluid flow and focused shear zone flow (Ague 2003) are shown by dotted lines. The range of partial vein filling (100 to 1 vol% of precipitating phase) is indicated by gray areas. Line styles are as in Fig. 8.

Mass transfer and mineral mobility in the Earth's interior

The present thermodynamic model provides a self-consistent formulation of all thermodynamic properties of mineral dissolution equilibria and their pressure and temperature dependence. We illustrate its utility by calculating the intensity of mass transfer and metasomatism and the related integrated fluid fluxes in several representative settings. Transport theory (see Appendix B) was applied to the calculation of the time-integrated fluid fluxes necessary to precipitate a unit volume of vein material (1 m^3). The integrated fluid fluxes for mineral precipitation along the geothermal gradients of 20 and 7°C km^{-1} are very similar, but vary significantly with temperature. They range from 10^7–10^{15} m^3 m^{-2} at 200°C to 10^4–10^8 m^3 m^{-2} at 1100°C (Fig. 10). When compared with characteristic integrated fluid fluxes during diffusive metamorphic flow and in crustal shear zones (Ferry 1994; Ague 2003), medium- to high-grade metamorphic temperatures are sufficient to cause substantial mobility of quartz, calcite and fluorite (in decreasing order; Fig. 10). Conversely, a predefined integrated fluid flux may be used to calculate and compare the magnitudes of mass transfer (in volume fraction precipitated or dissolved; Fig. 11). Along the geotherms and at a
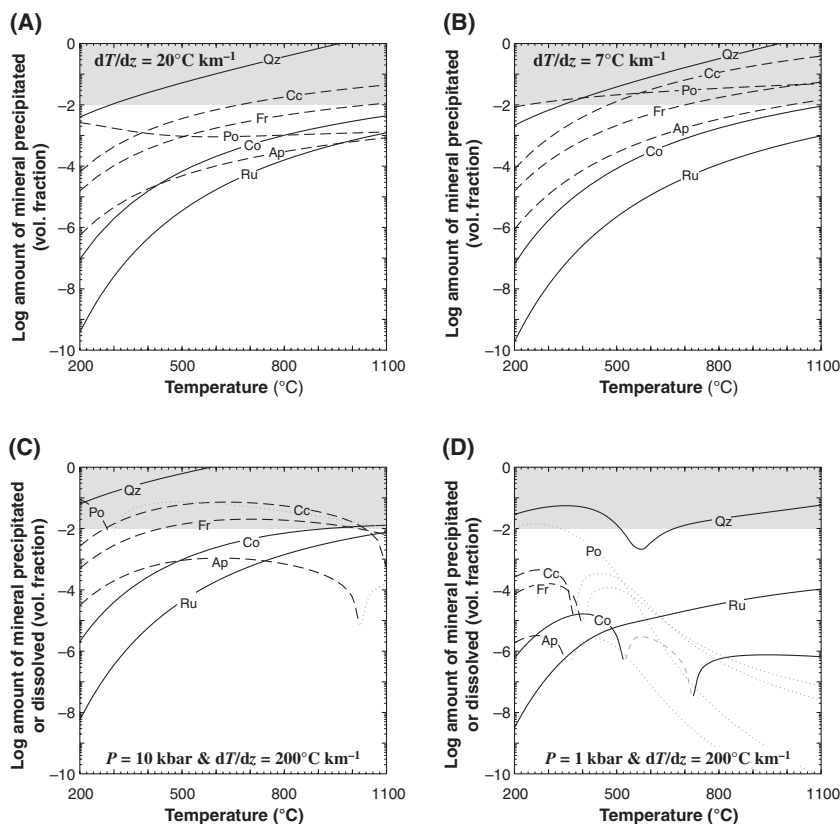
Fig. 11. Amount of precipitated or dissolved minerals produced by the integrated fluid flux, $q = 10^5$ m^3 m^{-2} (Ague 2003) at geothermal gradients of (A) 20 and (B) 7°C km^{-1}, and at constant pressure of (C) 10 and (D) 1 kbar. Mineral precipitation (as temperature decreases) is indicated by black curves, whereas dissolution is shown by gray dashed and dotted patterns. Gray area indicates a range between 1 and 100 vol% in the rock. Line styles are as in Fig. 8.

constant pressure of 10 kbar, the integrated fluid flux characteristic for metamorphic shear zones (10^5 m^3 m^{-2}; Ague 2003) leads to mobilities of SiO$_2$ from 1 vol% at 300–350°C to 10 vol% at 600–620°C and a complete silicification above 900°C. This is in good agreement with macroscopic observation of quartz segregations and veining from greenschist facies conditions. The fluid-mediated mobilities of calcite are one-half to one order of magnitude lower, but metasomatism of fluorite and apatite components may reach vol% levels at the highest subduction temperatures (Fig. 11b). Amounts of precipitation of rutile and corundum are low, from sub-ppm (at 200°C) to a few tenths of vol% (at 1100°C) but, importantly, these values are probably still significant for trace element redistribution during metamorphic events, focused fluid flow, or hydrothermal alteration.

During lateral fluid flow at constant pressure the extent of the mineral precipitation is expected to vary along the cooling path, or precipitation will alternate with mineral dissolution and loss in certain temperature segments (Fig. 11C, D). At 10 kbar, retrograde solubility occurs for portlandite above 290°C and above 1000°C for apatite. Other Ca-bearing phases such as calcite or fluorite variably precipitate during cooling (2–7 vol%), whereas the capability of oxide precipitation (quartz, corundum and rutile) strongly decreases with decreasing temperature. At 1 kbar, all minerals except rutile exhibit rapid changes in

precipitation and/or dissolution as a function of temperature (Fig. 11D). The intensity of silicification drops to below 1 vol% between 700 and 400°C, whereas corundum will dissolve between 720 and 530°C bracketed by precipitation at high or low temperatures. No Ca-bearing minerals precipitate above 390°C.

These results are applicable to spatial hydrothermal zoning in the vicinity of upper crustal intrusions. The intensity of silicification varies by nearly two orders of magnitude and quartz veining is expected to be most intense at 300–400°C. The behavior of aluminum, as judged from the corundum solubility, reverses from precipitation and dissolution, and back, which will probably enhance its local redistribution and hence mobility. Carbonates will not precipitate in high-temperature contact aureoles even if the fluids are CO$_2$ bearing, which promotes, by extrapolation, the formation of skarns replacing carbonate host rocks.

Limitations and extensions of the modeling

Our mass transport calculations illustrate the applicability and versatility of a density-based model to investigate fluid-mediated mass transfer in the Earth's crust and upper mantle. The results also highlight some limitations that stem from focusing only on congruent dissolution equilibria in pure water in the modeling. For example, for phases where the fluid–mineral interaction is controlled by the

formation of additional species or complexing, our calculations provide a minimum estimate of the mass transfer (that is, the amount of mineral precipitated or dissolved) or a maximum estimate for the integrated fluid flux. These observations indicate that, if formed under local equilibrium, metamorphic veins containing sparingly soluble minerals such as kyanite or rutile require either enormously large fluid fluxes or the presence of complexing agents, such as, halide, carbonate or aluminosilicate ligands and their polymeric successors (Tagirov & Schott 2001; Manning 2007; Antignano & Manning 2008b). The magnitude of this effect can be quantified by considering that $\partial \log m / \partial z$ is approximately independent of the nature of the mineral (Fig. 8); hence, the integrated fluid flux scales in direct proportion to the solubility increase in the presence of other aqueous complexes. The presence of 10 wt% dissolved silicates lowers the necessary fluid flux for rutile crystallization by a factor of 13 at 900°C and 10 kbar, or the quartz saturation enhance the kyanite precipitation by a factor of 6 at 700°C and 10 kbar. This brings the mobility of Ti and Al to wt% level at the highest temperatures modeled in this study (Fig. 11). Increasing self-dissociation of H_2O at high pressures and the presence of other complexing ions also play important roles.

CONCLUSIONS

(1) We have developed a new thermodynamic model for dissolution of minerals in aqueous fluids at high temperatures and pressures. The model incorporates thermodynamic contributions from lattice breakdown, ionization and hydration, which depend on temperature, and the effects associated with the compression in the hydration sphere and electrostatic solute–solvent interactions, which are formulated as a function of solvent volumetric properties. The solvent density term has the form of the generalized Krichevskii parameter, which is a finite and smooth function near the critical point of water, and has a simple linear scaling with the reciprocal dielectric constant.

(2) Experimental solubilities of seven rock-forming minerals were used to calibrate the model and demonstrate its performance. With the exception of quartz, solubilities in aqueous fluids at metamorphic and magmatic conditions can be described by three parameters to within the experimental scatter or accuracy. The solubility of quartz required a five-parameter formulation, which includes heat capacity and its temperature dependence. We propose that these terms probably assimilate the distinct enthalpy and entropy of the silica monomer and dimer, respectively, and/or deviations from the infinite-dilution limiting behavior as fluids become solute rich.

(3) Solubilities of all seven rock-forming minerals increase smoothly with temperature along metamorphic geotherms or water isochores. Temperature dependence is fairly similar for all solid phases but portlandite. The solubility of a given phase increases for a given phase by three to seven orders of magnitudes as temperature rises from 200 to 1100°C along typical geotherms. At constant pressure, however, mineral solubilities initially increase with rising temperature but subsequently drop. This effect is caused by a reversal in isobaric expansivity of the aqueous solvent, which propagates into the enthalpy of dissolution. The onset of retrograde solubility typically occurs at 300–400°C and it is a characteristic of all minerals.

(4) Solute speciation, volume of dissolution and the prograde–retrograde solubility behavior are inter-related. Oxide minerals such as quartz, corundum and rutile, which dissolve as predominantly neutral species, exhibit very small dependence on the solvent properties. Consequently, their isobaric retrograde solubility is limited to pressures below 1.3 kbar. The Ca-bearing phases, by contrast, produce variably charged species upon dissolution, where the electrostriction effects are more significant. Calcite, fluorite, apatite and portlandite show a decrease in mineral solubility at medium to high metamorphic grades over a wide range of pressures.

(5) Application of solute transport theory to our thermodynamic model permits calculation of time-integrated fluid fluxes, which are necessary to precipitate mineral veins during metamorphic events. The integrated fluid fluxes along geotherms of 20 and 7°C km^{-1} vary from 10^4 to 10^{15} m^3 m^{-2} in the following sequence: quartz, calcite, fluorite, corundum and apatite, and rutile. This is in broad agreement with observations of high mobility and veining of quartz and calcite as the most mobile-predicted phases in many metamorphic environments. Conversely, typical integrated fluid fluxes in crustal shear zones produce a transfer of quartz and calcite in quantities of several tens of vol%, whereas the solubility of apatite or rutile lies below 1000 ppm, which may still be important for the trace element budget in metasomatized rocks.

(6) The small number of parameters in the thermodynamic model allows correlation with the standard thermodynamic properties at arbitrary reference conditions (e.g. 25°C and 1 bar), which are readily available. In the appendix A we provide relationships for transformation of standard enthalpies, entropies, volumes and heat capacities into the model parameters. This approach enables utilization of existing thermodynamic data (e.g. the Helgeson–Kirkham–Flowers equation of state) in the framework of our model and allows extrapolation of standard thermodynamic properties over a wide range of metamorphic and magmatic temperatures and pressures.

REFERENCES

Ague JJ (1994) Mass transfer during Barrovian metamorphism of pelites, south-central Connecticut. I. Evidence for changes in composition and volume. *American Journal of Science*, **294**, 989–1057.

Ague JJ (1998) Simple models of coupled fluid infiltration and redox reactions in the crust. *Contributions to Mineralogy and Petrology*, **132**, 180–97.

Ague JJ (2003) Fluid flow in the deep crust. In: *Treatise of Geochemistry, v. 3: The crust* (ed. Rudnick RL), pp. 195–228. Elsevier, Amsterdam.

Akinfiev NN (2001) Equation of state of SiO_{2aq} for description of silica dissolution at temperatures of 0–600°C and pressures of 1–1000 bar. *Geochemistry International*, **39**, 1242–4.

Akinfiev NN, Diamond LW (2003) Thermodynamic description of aqueous nonelectrolytes at infinite dilution over a wide range of state parameters. *Geochimica et Cosmochimica Acta*, **67**, 613–27.

Akinfiev NN, Diamond LW (2004) A three-parameter EOS to describe aqueous non-electrolytes at infinite dilution over a wide range of state parameters, with preliminary application to 1:1 electrolytes. *Fluid Phase Equilibria*, **222/223**, 31–37.

Akinfiev NN, Diamond LW (2009) A simple predictive model of quartz solubility in water-salt-CO_2 systems at temperatures up to 1000°C and pressures up to 1000 MPa. *Geochimica et Cosmochimica Acta*, **73**, 1597–608.

Anderson GM (2005) *Thermodynamics of Natural Systems*, 2nd edn. Cambridge University Press, Cambridge.

Anderson GM, Burnham CW (1965) The solubility if quartz in supercritical water. *American Journal of Science*, **263**, 494–511.

Anderson GM, Castet S, Schott J, Mesmer RE (1991) The density model for estimation of thermodynamic parameters of reactions at high temperatures and pressures. *Geochimica et Cosmochimica Acta*, **55**, 1769–79.

Angell CA (1983) Supercooled water. *Annual Review in Physical Chemistry*, **34**, 593–630.

Antignano A, Manning CE (2008a) Fluorpatite solubility in H_2O and H_2O–NaCl at 700 to 900°C and 0.7 to 2.0 GPa. *Chemical Geology*, **251**, 112–9 & **255**, 294.

Antignano A, Manning CE (2008b) Rutile solubility in H_2O, H_2O–SiO_2, and H_2O–$NaAlSi_3O_8$ fluids at 0.7–2.0 GPa and 700–1000°C: implications for mobility of nominally insoluble elements. *Chemical Geology*, **255**, 283–93.

Armellini FJ, Tester JW (1993) Solubility of sodium chloride and sulfate in sub- and supercritical water vapor from 450–500°C and 100–250 bar. *Fluid Phase Equilibria*, **84**, 123–42.

Atkins PW, MacDermott AJ (1982) The Born equation and ionic solvation. *Journal of Chemical Education*, **59**, 359–60.

Audétat A, Keppler H (2005) Solubility of rutile in subduction zones fluids, as determined by experiments in the hydrothermal diamond anvil cell. *Earth and Planetary Science Letters*, **232**, 393–402.

Ayers JC, Watson EB (1993) Rutile solubility and mobility in supercritical aqueous fluids. *Contributions to Mineralogy and Petrology*, **114**, 321–30.

Baatartsogt B, Schwinn G, Wagner T, Taubald H, Beitter T, Markl G (2007) Contrasting paleofluid systems in the continental basement: a fluid inclusion and stable isotope study of hydrothermal vein mineralization, Schwarzwald district, Germany. *Geochimica et Cosmochimica Acta*, **64**, 123–47.

Bandura AV, Lvov SN (2006) The ionization constant of water over wide ranges of temperature and density. *Journal of Physical and Chemical Reference Data*, **35**, 15–30.

Baumgartner LP, Ferry JM (1991) A model for coupled fluid-flow and mixed-volatile mineral reactions with applications to regional metamorphism. *Contributions to Mineralogy and Petrology*, **106**, 273–85.

Bear J (1972) *Dynamics of Fluids in Porous Media*. Elsevier, New York.

Becker KH, Cemič L, Langer KEOE (1983) Solubility of corundum in supercritical water. *Geochimica et Cosmochimica Acta*, **47**, 1573–8.

Ben-Amotz D, Raineri FO, Stell G (2005) Solvation thermodynamics: theory and applications. *Journal of Physical Chemistry B*, **109**, 6866–78.

Ben-Naim A (2006) *Molecular Theory of Solutions*. Oxford University Press, Oxford.

Borg RJ, Dienes GJ (1992) *The Physical Chemistry of Solids*. Academic Press Inc., Boston, MA.

Born M (1920) Volumen und Hydratationswärme der Ionen. *Zeitschrift für Physik*, **1**, 45–8.

Bourcier WL, Knauss KG, Jackson KJ (1993) Aluminum hydrolysis constants to 250°C from boehmite solubility measurements. *Geochimica et Cosmochimica Acta*, **57**, 747–62.

Caciagli NC, Manning CE (2003) The solubility of calcite in water at 5–16 kar and 500–800°C. *Contributions to Mineralogy and Petrology*, **146**, 275–85.

Clarke R, Hnědkovský L, Tremaine PR, Majer V (2000) Amino acids under hydrothermal conditions: apparent molar heat capacities of aqueous α-alanine, β-alanine, glycine, and proline at temperature from 298 to 500 K and pressures up to 30.0 MPa. *Journal of Physical Chemistry B*, **104**, 11781–93.

Cooney WJ, O'Connell JP (1987) Correlation of partial molar volumes at infinite dilution of salts in water. *Chemical Engineering Communications*, **56**, 341–7.

Crerar DA, Anderson GM (1971) Solubility and solvation reactions of quartz in dilute hydrothermal solutions. *Chemical Geology*, **8**, 107–22.

Crovetto R, Wood RH, Majer V (1991) Revised densities of ($xCO_2 + (1 - x)H_2O$) with $x < 0.014$ at supercritical conditions: molar volumes, partial molar volumes of CO_2 at infinite dilution, and excess molar volumes. *Journal of Chemical Thermodynamics*, **23**, 1139–46.

Dolejš D, Wagner T (2008) Thermodynamic modeling of non-ideal mineral–fluid equilibria in the system Si–Al–Fe–Mg–Ca–Na–K–H–O–Cl at elevated temperatures and pressures: implications for hydrothermal mass transfer in granitic rocks. *Geochimica et Cosmochimica Acta*, **72**, 526–53.

Ellis AJ (1966) Partial molal volumes of alkali chlorides in aqueous solution to 200°. *Journal of Chemical Society (A)*, **1966**, 1579–84.

Eugster HP, Baumgartner LP (1987) Mineral solubilities and speciation in supercritical metamorphic fluids. *Reviews in Mineralogy*, **17**, 367–403.

Fein J, Walther JV (1989) Calcite solubility and speciation in supercritical NaCl–HCl aqueous fluids. *Contributions to Mineralogy and Petrology*, **103**, 317–24.

Fernandéz DP, Goodwin AR, Lemmon EW, Levelt Sengers JMH, Williams RC (1997) A formulation for the static permittivity of

water and steam at temperatures from 238 K to pressures up to 1200 MPa, including derivatives and Debye–Hückel coefficients. *Journal of Physical and Chemical Reference Data*, **26**, 1125–66.

Ferry JM (1994) Overview of the petrological record of fluid flow during regional metamorphism in northern New England. *American Journal of Science*, **294**, 905–88.

Ferry JM, Burt DM (1982) Characterization of metamorphic fluid composition through mineral equilibria. *Reviews in Mineralogy*, **10**, 207–62.

Ferry JM, Dipple GM (1991) Fluid flow, mineral reactions, and metasomatism. *Geology*, **19**, 211–4.

Ferry JM, Gerdes ML (1998) Chemically reactive fluid flow during metamorphism. *Annual Review of Earth and Planetary Sciences*, **26**, 255–87.

Fletcher P (1993) *Chemical Thermodynamics for Earth Scientists*. Longman Scientific & Technical, Harlow.

Fournier RO (1983) A method for calculating quartz solubilities in aqueous sodium chloride solutions. *Geochimica et Cosmochimica Acta*, **47**, 579–86.

Fournier RO (1999) Hydrothermal processes related to movement of fluid from plastic into brittle rock in the magmatic-epithermal environment. *Economic Geology*, **94**, 1193–212.

Fournier RO, Marshall WL (1983) Calculation of amorphous silica solubilities at 25° to 300°C and apparent cation hydration numbers in aqueous salt solutions using the concept of effective density of water. *Geochimica et Cosmochimica Acta*, **47**, 587–96.

Fournier RO, Potter RW, II (1982) An equation correlating the solubility of quartz in water from 25° to 900°C at pressures up to 10,000 bars. *Geochimica et Cosmochimica Acta*, **46**, 1969–73.

Franck EU (1956a) Hochverdichteter Wasserdampf III. Ionendissoziation von HCl, KOH und H_2O im überkritischem Wasser. *Zeitschrift für Physikalische Chemie, Neue Folge*, **8**, 192–206.

Franck EU (1956b) Zur Löslichkeit fester Stoffe in verdichteten Gasen. *Zeitschrift für Physikalische Chemie, Neue Folge*, **6**, 345–55.

Franck EU, Rosenzweig S, Christoforakos M (1990) Calculation of the dielectric constant of water to 1000°C and very high pressures. *Berichte der Bunsen-Gesellschaft*, **94**, 199–203.

Frantz JD, Marshall WL (1982) Electrical conductances and ionization constants of $CaCl_2$ and $MgCl_2$ in aqueous solutions at temperatures to 600°C and pressures to 4000 bars. *American Journal of Science*, **282**, 1666–93.

Galobardes JV, Van Hare DR, Rogers LB (1981) Solubility of sodium chloride in dry steam. *Journal of Chemical Engineering Data*, **26**, 363–5.

Gerya TV, Maresch WV, Burchard M, Zakhartchouk V, Doltsinis NL, Fockenberg T (2005) Thermodynamic modeling of solubility and speciation of silica in H_2O–SiO_2 fluid up to 1300°C and 20 kbar based on the chain reaction formalism. *European Journal of Mineralogy*, **17**, 269–83.

Hamann SD, Lim SC (1954) The volume changes on ionization of weak electrolytes. *Australian Journal of Chemistry*, **7**, 329–34.

Hanson RB (1992) Effects of fluid production on fluid flow during regional and contact metamorphism. *Journal of Metamorphic Geology*, **10**, 87–97.

Harvey AH (1998) *Thermodynamic Properties of Water: Tabulation from the IAPWS Formulation 1995 for the Thermodynamic Properties of Ordinary Water Substance for General and Scientific Use*. NIST Internal Report 5078.

Helgeson HC, Kirkham DH (1974) Theoretical prediction of the thermodynamic behavior of aqueous electrolytes at high pressures and temperatures. I. Summary of the thermodynamic/electrostatic properties of the solvent. *American Journal of Science*, **274**, 1089–198.

Helgeson HC, Kirkham D, Flowers GC (1981) Thermodynamic behavior of aqueous electrolytes at high pressures and temperatures. IV. Calculation of activity coefficients, osmotic coefficients, and apparent molal and standard and relative partial molal properties to 600°C and 5 kb. *American Journal of Science*, **281**, 1249–516.

Hemley JJ, Montoya JW, Marinenko JW, Luce RW (1980) Equilibria in the system Al_2O_3–SiO_2–H_2O and some general implications for alteration/mineralization processes. *Economic Geology*, **75**, 210–28.

Higashi H, Iwai Y, Matsumoto K, Kitani Y, Okazaki F, Shimoyama Y, Arai Y (2005) Measurement and correlation for solubilities of alkali metal chlorides in water vapor at high temperature and pressure. *Fluid Phase Equilibria*, **228/229**, 547–551.

Hillert M (2008) *Phase Equilibria, Phase Diagrams and Phase Transformations. Their Thermodynamic Basis*, 2nd edn. Cambridge University Press, Cambridge.

Holland TJB, Powell R (1998) An internally consistent thermodynamic data set for phases of petrological interest. *Journal of Metamorphic Geology*, **16**, 309–43.

Hummel W, Berner U, Curti E, Pearson FJ, Thoenen T (2002) *Nagra/PSI Chemical Thermodynamic Database 01/01*. Universal Publishers, Parkland, FL.

Jamtveit B, Yardley B (Eds) (1997) *Fluid Flow and Transport in Rocks*. Chapman & Hall, London.

Johnson JW, Oelkers EH, Helgeson HC (1992) SUPCRT92: a software package for calculating the standard molal thermodynamic properties of minerals, gases, aqueous species, and reactions from 1 to 5000 bar and 0 to 1000°C. *Computers & Geosciences*, **18**, 899–947.

Kebarle P (1977) Ion thermochemistry and solvation from gas phase ion equilibria. *Annual Review of Physical Chemistry*, **28**, 445–76.

Kennedy GC (1950) A portion of the system silica-water. *Economic Geology*, **45**, 629–53.

Kirkwood JG, Buff FP (1951) The statistical mechanical theory of liquids. *Journal of Chemical Physics*, **19**, 774–82.

Kitahara S (1960) The solubility equilibrium and the rate of solution of quartz in water at high temperatures and high pressures. *Review of Physical Chemistry of Japan*, **30**, 122–30.

Knauss KG, Dibley MJ, Bourcier WL, Shaw HF (2001) Ti(IV) hydrolysis constants derived from rutile solubility measurements made from 100 to 300°C. *Applied Geochemistry*, **16**, 1115–28.

Levelt Sengers JMH (1991) Solubility near the solvent's critical point. *Journal of Supercritical Fluids*, **4**, 215–22.

Mackie PE, Young RA (1974) Fluorine-chlorine interaction in fluor-chlorapatite. *Journal of Solid State Chemistry*, **11**, 319–29.

Maclean WH (1990) Mass change calculations in altered rock series. *Mineralium Deposita*, **25**, 44–9.

Maclean WH, Barrett TJ (1993) Lithogeochemical technique using immobile elements. *Journal of Geochemical Exploration*, **48**, 109–33.

Majer V, Sedlbauer J, Bergin G (2008) Henry's law constant and related coefficients for aqueous hydrocarbons, CO_2 and H_2S over a wide range of temperature and pressure. *Fluid Phase Equilibria*, **272**, 65–74.

Mangas J, Arribas A (1987) Fluid inclusion study in different types of tin deposits associated with the Hercynian granites of western Spain. *Chemical Geology*, **61**, 193–208.

Manning CE (1994) The solubility of quartz in H_2O in the lower crust and upper mantle. *Geochimica et Cosmochimica Acta*, **58**, 4831–9.

Manning CE (2007) Solubility of corundum + kyanite in H_2O at 700°C and 10 kbar: evidence for Al–Si complexing at high pressure and temperature. *Geofluids*, **7**, 258–69.

Manning CE, Wilke M, Schmidt C, Cauzid J (2008) Rutile solubility in albite–H_2O and $Na_2Si_3O_7$–H_2O at high temperatures and pressures by in-situ synchrotron radiation micro-XRF. *Earth and Planetary Science Letters*, **272**, 730–7.

Manning CE, Antignano A, Lin HA (2010) Premelting polymerization of crustal and mantle fluids, as indicated by solubility of albite + paragonite + quartz in H_2O at 1 GPa and 350–620°C. *Earth and Planetary Science Letters*, **292**, 325–36.

Marshall WL (2008a) Dielectric constant of water discovered to be simple function of density over extreme ranges from −35 to +600°C and to 1200 MPa (12000 Atm.), believed universal. *Nature Precedings*, doi: 10.1038/npre.2008.2472.1, 1–40.

Marshall WL (2008b) Aqueous electrolyte ionization over extreme ranges as simple fundamental relation with density and believed universal; sodium chloride ionization from 0° to 1000°C and to 1000 MPa (10000 Atm.). *Nature Precedings*, hdl:10101/npre.2008.2476.1, 1–40.

Marshall WL, Franck EU (1981) Ion product of water substance, 0–1000 °C, 1–10,000 bars. New international formulation and its background. *Journal of Physical and Chemical Reference Data*, **10**, 295–304.

Marshall WL, Quist AS (1967) A representation of isothermal ion–ion-pair-solvent equilibria independent of changes in dielectric constant. *Proceedings of the National Academy of Sciences*, **58**, 901–6.

Martynova OI (1964) Some problems of the solubility of involatile inorganic compounds in water vapour at high temperatures and pressures. *Russian Journal of Physical Chemistry*, **38**, 587–92.

McKenzie WF, Helgeson HC (1984) Estimation of the dielectric constant of H_2O from experimental solubilities of quartz, and calculation of the thermodynamic properties of aqueous species to 900°C at 2 kbar. *Geochimica et Cosmochimica Acta*, **48**, 2167–77.

Megaw HD (1933) The thermal expansions of certain crystals with layer lattices. *Proceedings of the Royal Society London A*, **142**, 198–214.

Mehnert LD, Dipple GM, Nicolescu S (2005) World skarn deposits. *Economic Geology*, **100th Anniversary Volume**, 299–336.

Mesmer RE, Marshall WL, Palmer DA, Simonson JM, Holmes HF (1988) Thermodynamics of aqueous association at high temperatures and pressures. *Journal of Solution Chemistry*, **17**, 699–718.

Mesmer RE, Palmer DA, Simonson JM (1991) Ion association at high temperatures and pressures. In: *Activity Coefficients in Electrolyte Solutions*, 2nd edn (ed. Pitzer KS), pp. 491–529. CRC Press, Boca Raton, FL.

Morey GW (1962) The action of water on calcite, magnesite and dolomite. *American Mineralogist*, **47**, 1456–60.

Morey GW, Hesselgesser JM (1951) The solubility of some minerals in superheated steam at high pressures. *Economic Geology*, **46**, 821–35.

Morey GW, Fournier RO, Rowe JJ (1962) The solubility of quartz in water in the temperature interval from 25° to 300°C. *Geochimica et Cosmochimica Acta*, **26**, 1029–43.

Mosebach R (1955) Die hydrothermale Löslichkeit des Quarzes als heterogenes Gasgleichgewicht. *Neues Jahrbuch für Mineralogie Abhandlungen*, **87**, 351–88.

Newton RC, Manning CE (2002) Solubility of silica in equilibrium with enstatite, forsterite, and H_2O at deep crust/upper mantle pressures and temperatures and an activity-coefficient model for polymerization of aqueous silica. *Geochimica et Cosmochimica Acta*, **66**, 4165–76.

Newton RC, Manning CE (2003) Activity coefficient and polymerization of aqueous silica at 800°C, 12 kbar, from solubility measurements on SiO_2-buffering mineral assemblages. *Contributions to Mineralogy and Petrology*, **146**, 135–43.

Newton RC, Manning CE (2008a) Thermodynamics of SiO_2–H_2O fluid near the upper critical end point from quartz solubility measurements at 10 kbar. *Earth and Planetary Science Letters*, **274**, 241–9.

Newton RC, Manning CE (2008b) Solubility of corundum in the system Al_2O_3–SiO_2–H_2O–NaCl at 800°C and 10 kbar. *Chemical Geology*, **249**, 250–61.

Nichols GT, Wiebe RA (1998) Desilication veins in the Cadillac Mountain granite (Maine, USA): a record of reversals in the SiO_2 solubility of H_2O-rich vapor released during subsolidus cooling. *Journal of Metamorphic Geology*, **16**, 795–808.

Norton DL, Dutrow BL (2001) Complex behavior of magma-hydrothermal processes: role of supercritical fluid. *Geochimica et Cosmochimica Acta*, **65**, 4009–17.

Norton DL, Knight JE (1977) Transport phenomena in hydrothermal systems: cooling plutons. *American Journal of Science*, **277**, 937–81.

O'Connell JP (1971) Thermodynamic properties of solutions based on correlation functions. *Molecular Physics*, **20**, 27–33.

O'Connell JP (1990) Thermodynamic properties of mixtures from fluctuation solution theory. In: *Fluctuation Theory of Mixtures* (eds Matteoli E, Mansoori GA), pp. 45–67. Taylor & Francis, New York.

O'Connell JP, Sharygin AV, Wood RH (1996) Infinite dilution partial molar volumes of aqueous solutes over wide ranges of conditions. *Industrial Engineering Chemistry Research*, **35**, 2808–12.

Oelkers EH, Helgeson HC, Shock EL, Sverjensky DA, Johnson JW, Pokrovskii VA (1995) Summary of the apparent standard partial molal Gibbs free energies of formation of aqueous species, minerals, and gases at pressures 1 to 5000 bars and temperatures 25 to 1000°C. *Journal of Physical and Chemical Reference Data*, **24**, 1401–560.

Parkhurst DL, Appelo CAJ (1999) *User's guide to PHREEQC (version 2) − a computer program for speciation, batch-reaction, one-dimensional transport, and inverse geochemical calculations*. Water-Resources Investigations Report 99-4259.

Pierotti RA (1963) The solubility of gases in liquids. *Journal of Physical Chemistry*, **67**, 1840–5.

Pierotti RA (1976) A scaled particle theory of aqueous and nonaqueous solutions. *Chemical Reviews*, **76**, 717–26.

Pina CM, Putnis A, Astilleros JM (2004) The growth mechanisms of solid solutions crystallising from aqueous solutions. *Chemical Geology*, **204**, 145–61.

Pitzer KS (1982) Self-ionization of water at high-temperature and the thermodynamic properties of the ions. *Journal of Physical Chemistry*, **86**, 4704–8.

Pitzer KS (1983a) Thermodynamics of sodium chloride solutions in steam. *Journal of Physical Chemistry*, **87**, 1120–5.

Pitzer KS (1983b) Dielectric constant of water at very high temperature and pressure. *Proceedings of the National Academy of Sciences*, **80**, 4575–6.

Plyasunov AV (1993) Description of the standard thermodynamic properties of dissolved electrolytes from the total equilibrium constant. *Geochemistry International*, **30**, 52–65.

Plyasunov AV, O'Connell JP, Wood RH (2000) Infinite dilution partial molar properties of aqueous solutions of nonelectrolytes. I. Equations for partial molar volumes at infinite dilution and standard thermodynamic functions of hydration of volatile nonelectrolytes over wide ranges of conditions. *Geochimica et Cosmochimica Acta*, **64**, 495–512.

Pokrovski GS, Roux J, Harrichoury JC (2005a) Fluid density control on vapor-liquid partitioning of metals in hydrothermal systems. *Geology*, **33**, 657–60.

Pokrovski GS, Roux J, Hazemann JL, Testemale D (2005b) An X-ray absorption spectroscopy study of argutite solubility and aqueous Ge(IV) speciation in hydrothermal fluids to 500 °C and 400 bar. *Chemical Geology*, **217**, 127–45.

Pokrovski GS, Borisova AYu, Harrichoury JC (2008) The effect of sulfur on vapor–liquid fractionation of metals in hydrothermal systems. *Earth and Planetary Science Letters*, **266**, 345–62.

Putnis A, Putnis CV (2007) The mechanism of reequilibration of solids in the presence of a fluid phase. *Journal of Solid State Chemistry*, **180**, 1783–6.

Quist AS (1970) The ionization constant of water to 800°C and 4000 bars. *Journal of Physical Chemistry*, **74**, 3393–402.

Quist AS, Marshall WL (1968) Electrical conductances of aqueous sodium chloride solutions from 0 to 800° and at pressures to 4000 bars. *Journal of Physical Chemistry*, **72**, 684–703.

Ragnarsdóttir KV, Walther JV (1985) Experimental determination of corundum solubilities in pure water between 400–700°C and 1–3 kbar. *Geochimica et Cosmochimica Acta*, **49**, 2109–15.

Reed M (1997) Hydrothermal alteration and its relationship to ore fluid composition. In: *Geochemistry of Hydrothermal Ore Deposits*, 3rd edn (ed. Barnes HL), pp. 303–65. John Wiley & Sons, New York.

Rimstidt JD (1997) Quartz solubility at low temperatures. *Geochimica et Cosmochimica Acta*, **61**, 2553–8.

Ryzhenko BN, Kovalenko NI, Prisyagina NI (2006) Titanium complexation in hydrothermal systems. *Geochemistry International*, **44**, 879–95.

Scambelluri M, Fiebig J, Malaspina N, Müntener O, Pettke T (2004) Serpentinite subduction; implications for fluid processes and trace-element recycling. *International Geology Review*, **46**, 595–613.

Schloemer VH (1952) Hydrothermale untersuchungen über das system CaO–MgO–CO₂–H₂O. *Neues Jahrbuch für Mineralogie Monatshefte*, **1952**, 129–35.

Sedlbauer J, Wood RH (2004) Thermodynamic properties of dilute NaCl(aq) solutions near the critical point of water. *Journal of Physical Chemistry B*, **108**, 11838–49.

Sedlbauer J, O'Connell JP, Wood RH (2001) A new equation of state for correlation and prediction of standard molal thermodynamic properties of aqueous species at high temperatures and pressures. *Chemical Geology*, **163**, 43–63.

Shock EL, Helgeson HC (1988) Calculation of the thermodynamic and transport properties of aqueous species at high pressures and temperatures: Correlation algorithms for ionic species and equation of state predictions to 5 kb and 1000°C. *Geochimica et Cosmochimica Acta*, **52**, 2009–36.

Shock EL, Oelkers EH, Johnson JW, Sverjensky DA, Helgeson HC (1992) Calculation of the thermodynamic properties of aqueous species at high pressures and temperatures: effective electrostatic radii, dissociation constants and standard partial molal properties to 1000°C and 5 kbar. *Journal of the Chemical Society, Faraday Transactions*, **88**, 803–26.

Spandler C, Hermann J (2006) High-pressure veins in eclogite from New Caledonia and their significance for fluid migration in subduction zones. *Lithos*, **89**, 135–53.

Speziale S, Duffy TS (2002) Single-crystal elastic constants of fluorite (CaF₂) to 9.3 GPa. *Physics and Chemistry of Minerals*, **29**, 465–72.

Strübel G (1965) Quantitative Untersuchungen über die hydrothermale Löslichkeit von Flußspat (CaF₂). *Neues Jahrbuch für Mineralogie, Monatshefte*, **1965**, 83–95.

Sue K, Adschiri T, Arai K (2002) Predictive model for equilibrium constants of aqueous inorganic species at subcritical and supercritical conditions. *Industrial Engineering and Chemistry Research*, **41**, 3298–306.

Sverjensky DA, Shock EL, Helgeson HC (1997) Prediction of the thermodynamic properties of aqueous metal complexes to 1000°C and 5 kb. *Geochimica et Cosmochimica Acta*, **61**, 1359–412.

Sweeton FH, Mesmer RE, Baes CF Jr (1974) Acidity measurements at elevated temperatures. VII. Dissociation of water. *Journal of Solution Chemistry*, **3**, 191–214.

Tagirov B, Schott J (2001) Aluminum speciation in crustal fluids revisited. *Geochimica et Cosmochimica Acta*, **65**, 3965–92.

Tanger JC IV, Helgeson HC (1988) Calculation of the thermodynamic and transport properties of aqueous species at high pressures and temperatures: revised equations of state for the standard partial molal properties of ions and electrolytes. *American Journal of Science*, **288**, 19–98.

Tanger JC IV, Pitzer KS (1989a) Calculation of the ionization constant of H₂O to 2,273 K and 500 MPa. *AIChE Journal*, **35**, 1631–8.

Tanger JC IV, Pitzer KS (1989b) Calculation of the thermodynamic properties of aqueous electrolytes to 1000°C and 5000 bar from a semicontinuum model for ion hydration. *Journal of Physical Chemistry*, **93**, 4941–51.

Thompson AB (1997) Flow and focusing of metamorphic fluids. In: *Fluid Flow and Transport in Rocks* (eds Jamtveit B, Yardley BWD), pp. 297–314. Chapman & Hall, London.

Tremaine PR, Shvedov D, Xiao C (1997) Thermodynamic properties of aqueous morpholine and morpholinium chloride at temperatures from 10 to 300°C: apparent molar volumes, heat capacities, and temperature dependence of ionization. *Journal of Physical Chemistry B*, **101**, 409–19.

Tremaine P, Zhang K, Benezeth P, Xiao C (2004) Ionization equilibria of acids and basis under hydrothermal conditions. In: *Aqueous Systems at Elevated Temperatures and Pressures. Physical Chemistry in Water, Steam and Hydrothermal Solutions* (eds Palmer DA, Fernández-Prini R, Harvey AH), pp. 441–92. Elsevier, Amsterdam.

Tropper P, Manning CE (2005) Very low solubility of rutile in H₂O at high pressure and temperature, and its implications for Ti mobility in subduction zones. *American Mineralogist*, **90**, 502–5.

Tropper P, Manning CE (2007a) The solubility of corundum in H₂O at high pressure and temperature and its implications for Al mobility in the deep crust and upper mantle. *Chemical Geology*, **240**, 54–60 & **248**, 114.

Tropper P, Manning CE (2007b) The solubility of fluorite in H₂O and H₂O–NaCl at high pressure and temperature. *Chemical Geology*, **242**, 299–306.

Vasilev VP, Vorobev PN, Khodakovskii IL (1974) Standard free energies of formation of titanium hydroxocomplexes and of the

Ti^{4+} ion in aqueous solution. *Russian Journal of Inorganic Chemistry*, **19**, 1481–3.

Vernon RH, Clarke GL (2008) *Principles of Metamorphic Petrology*. Cambridge University Press, Cambridge.

Wagman DD, Evans WH, Parker VB, Schumm RH, Halow I, Bailey SM, Churney KL, Nuttall RL (1982) The NBS tables of chemical thermodynamic properties. Selected values for inorganic and C1 and C2 organic substances in SI units. *Journal of Physical and Chemical Reference Data*, **11** (Suppl. 2), 1–392.

Wagner W, Pruß A (2002) The IAPWS formulation 1995 for the thermodynamic properties of ordinary water substance for general and scientific use. *Journal of Physical and Chemical Reference Data*, **31**, 387–535.

Walther JV (1986) Experimental determination of portlandite and brucite solubilities in supercritical H$_2$O. *Geochimica et Cosmochimica Acta*, **50**, 733–9.

Walther JV (1997) Experimental determination and interpretation of the solubility of corundum in H$_2$O between 350 and 600°C from 0.5 to 2.2 kbar. *Geochimica et Cosmochimica Acta*, **61**, 4955–64.

Walther JV, Helgeson HC (1977) Calculation of the thermodynamic properties of aqueous silica and the solubility of quartz and its polymorphs at high pressures and temperatures. *American Journal of Science*, **277**, 1315–51.

Walther JV, Long MI (1986) Experimental determination of calcite solubilities in supercritical H$_2$O. In: *Proceedings of the Fifth International Symposium on Water–Rock Interaction*. (ed Hitchon RB), pp. 609–11. National Energy Authority, Reykjavik, Iceland.

Walther JV, Orville P (1983) The extraction-quench technique for determination of the thermodynamic properties of solute complexes: application to quartz solubility in fluid mixtures. *American Mineralogist*, **68**, 731–41.

Wasserman E, Wood B, Brodholt J (1995) The static dielectric constant of water at pressures up to 20 kbar and temperatures to 1273 K: experiment, simulations, and empirical equations. *Geochimica et Cosmochimica Acta*, **59**, 1–6.

Weill DF, Fyfe WS (1964) The solubility of quartz in H$_2$O in the range 1000–4000 bars and 400–550°C. *Geochimica et Cosmochimica Acta*, **28**, 1243–55.

Widmer T, Thompson AB (2001) Local origin of high pressure vein material in eclogite facies rocks of the Zermatt–Saas Zone, Switzerland. *American Journal of Science*, **301**, 627–56.

Wood RH, Quint JR, Groller J-PE (1981) Thermodynamics of a charged hard sphere in a compressible dielectric fluid. A modification of the Born equation to include the compressibility of the solvent. *Journal of Physical Chemistry*, **85**, 3944–9.

Wood RH, Carter RW, Quint JR, Majer V, Thompson PT, Boccio JR (1994) Aqueous electrolytes at high temperatures: comparison of experiment with simulation and continuum models. *Journal of Chemical Thermodynamics*, **26**, 225–49.

Wyart J, Sabatier G (1955) Nouvelles mesures de la solubilité du quartz, de la tridymite et de la cristobalite dans l'eau sous pression au-dessus de la température critique. *Comptes Rendus de l'Académie des Sciences*, **240**, 1905–7.

Zack T, John T (2007) An evaluation of reactive fluid flow and trace element mobility in subducting slabs. *Chemical Geology*, **239**, 199–216.

Zemniak SE, Jones ME, Combs KE (1993) Solubility behavior of titanium(IV) oxide in alkaline media at elevated temperatures. *Journal of Solution Chemistry*, **22**, 601–23.

Zotov N, Keppler H (2000) In-situ Raman spectra of dissolved silica species in aqueous fluids to 900°C and 14 kbar. *American Mineralogist*, **85**, 600–3.

Zotov N, Keppler H (2002) Silica speciation in aqueous fluids at high pressures and high temperatures. *Chemical Geology*, **184**, 71–82.

APPENDIX. A

Thermodynamic equivalences

The new thermodynamic model in reduced form with three independent parameters can be calibrated using the standard thermodynamic properties of minerals and aqueous species at reference temperature and pressure, e.g. 25°C and 1 bar (e.g. Johnson *et al.* 1992; Oelkers *et al.* 1995). The three-parameter form,

$$\Delta_{ds}G = a + bT + eT \ln \rho, \tag{A1}$$

$$\ln K = -\frac{1}{R}\left\{\frac{a}{T} + b + e \ln \rho\right\}, \tag{A2}$$

requires that three independent thermodynamic properties must be known – $\Delta_{ds}G$ or $\Delta_{ds}H$, $\Delta_{ds}S$, and $\Delta_{ds}V$ or $\Delta_{ds}c_P$; note that volume and heat capacity are not independent (cf. Anderson *et al.* 1991). Using Eq. A1 and rearranging Eqs 16–19, the model parameters are obtained as follows:

$$e = \frac{\Delta_{ds}V}{\beta T} = \frac{\Delta_{ds}c_P}{2T\alpha_w + T^2(\partial\alpha_w/\partial T)_P}, \tag{A3}$$

$$b = -\Delta_{ds}S + e(T\alpha_w - \ln \rho_w), \tag{A4}$$

$$a = \Delta_{ds}H - eT^2\alpha_w = \Delta_{ds}G + T\Delta_{ds}S - eT^2\alpha_w. \tag{A5}$$

The above relationships can be used with the standard thermodynamic properties at any temperature and pressure by employing T and ρ, β, α and $(d\alpha/dT)_P$ of water at the preferred reference conditions (e.g. 25°C and 1 bar). The calibration provides means of predicting mineral solubilities (Eq. 14) at any temperature and pressure of interest.

APPENDIX. B

Transport theory

The transport theory is used to calculate amounts of solids precipitating from ascending aqueous fluids (Baumgartner & Ferry 1991; Ferry & Dipple 1991). In advection-reaction equation the mass conservation during porous isotropic flow is expressed as follows (e.g. Bear 1972, pp. 77–78; Ague 1998):

$$\frac{\partial c_i}{\partial t} = -v\frac{\partial c_i}{\partial x} + R_i \tag{B1}$$

where c is the molar concentration of solute i, t is time, x and v are the distance and flow velocity, respectively, and

R denotes the reaction rate. At steady state, which is closely approached during mineral-fluid buffering (Ferry & Burt 1982), the solute concentration is invariant with time, $\partial c_i/\partial t = 0$; hence,

$$R_i = \frac{\partial c_i}{\partial x} v. \tag{B2}$$

As mineralogical record in rocks reflects the time-integrated result of fluid–rock interaction, integrating Eq. B2 over time,

$$\int_0^t R_i \, dt = \int_0^t \frac{\partial c_i}{\partial x} v \, dt, \tag{B3}$$

leads to

$$n_i = \frac{q_V}{V} \frac{\partial m_i}{\partial z}, \tag{B4}$$

where n is the number of moles of i precipitated per rock volume, q_V is the time-integrated fluid, and V is the molar volume of aqueous fluid. The gradient of molality with vertical distance during one-dimensional flow, $\partial m_i/\partial z$, is recast into temperature and pressure dependence:

$$\frac{\partial m_i}{\partial z} = \frac{\partial m_i}{\partial T} \frac{\partial T}{\partial z} + \frac{\partial m_i}{\partial P} \frac{\partial P}{\partial z} \tag{B5}$$

where $\partial T/\partial z$ and $\partial T/\partial P$ represent the geothermal and pressure gradient of interest, whereas the molality changes with temperature and pressure are obtained from the standard thermodynamic properties of dissolution (cf. Eqs 17 and 19) as follows:

$$\frac{\partial m_i}{\partial T} = K \frac{\partial \ln K}{\partial T} = K \frac{\Delta_{ds} H}{RT^2}, \tag{B6}$$

$$\frac{\partial m_i}{\partial P} = K \frac{\partial \ln K}{\partial P} = -K \frac{\Delta_{ds} V}{RT}. \tag{B7}$$

These relationships illustrate that the amount of substance precipitated from 1 kg of aqueous fluid per temperature or pressure increment depends on *both* the solute concentration (expressed by $K = m$) and its gradient.